17

Volcanological Applications of Doppler Radars: A Review and Examples from a Transportable Pulse Radar in L-Band

Franck Donnadieu
[1]Clermont Université, Université Blaise Pascal, Observatoire de Physique du Globe de Clermont-Ferrand (OPGC), Laboratoire Magmas et Volcans, Clermont-Ferrand
[2]CNRS, UMR 6524, LMV, Clermont-Ferrand
[3]IRD, R 163, LMV, Clermont-Ferrand
France

1. Introduction

Many types of radar systems have been applied to the study of a wide range of volcanic features. Fields of application commonly include volcano deformation by interferometric synthetic aperture radar (InSAR), mainly satellite-based (e.g. Froger et al., 2007) but also ground-based like LISA (Casagli et al., 2009), digital elevation model generation using satellite or airborne InSAR measurements, surface products mapping by amplitude images of satellite radars, characterization of unexposed deposits by ground-penetrating radars (Russell & Stasiuk, 1997), monitoring of active lava domes and flows by either ad-hoc ground-based radars (e.g. Malassingne et al., 2001; Macfarlane et al., 2006; Wadge et al., 2005, 2008) or commercial ones (Hort et al., 2006; Vöge & Hort, 2008, 2009; Vöge et al., 2008), and quantitative characterization of explosive activity by means of fixed weather radars (large ash plumes) and transportable radars (Strombolian activity, weak ash plumes). A thorough review of all radar applications in volcanology is beyond the scope of this chapter which, instead, focuses on recent investigations of explosive eruptive regimes enhanced by the developments of dedicated transportable ground-based radars, by the recent advances made in signal interpretation using eruption models, and by the important concerns raised by ash plume hazards.

Below, weather and transportable radar systems used hitherto to monitor and study tephra emissions are first reviewed along with their advantages and limitations. Some differences relevant to the study of radar signals of volcanic origin are also described. Then I present a unique transportable pulse Doppler radar named VOLDORAD, operating in the L-band and dedicated to the study of explosive activity. Because it can be set up close to an eruptive vent and sound at a high rate the interior of even heavily particle-laden plumes within small beam volumes right above the emission source, many features of processes and dynamics of volcanic emissions can be characterized at different time scales from the spatiotemporal analysis of echo signals. Examples are provided of records obtained with VOLDORAD at

several volcanoes in different sounding conditions and various types of volcanic activity, from Strombolian lava jets to weak ash plumes. They are meant to illustrate the many capabilities of this type of radar and the interpretation of the variety of Doppler signatures in terms of volcanic processes.

2. Radar monitoring of explosive eruptions

2.1 Ash plume hazards and tephra dispersal forecast

Volcanic ash plumes generate important hazards as widespread ash fallout may cause serious perturbations to surrounding population and infrastructures. In addition, volcanic ash clouds derived from eruptive columns, even of moderate size, can generate direct hazards to aviation, as recently highlighted by the 2010 Eyjafjöll eruption in Iceland. The air traffic was disrupted over Europe for several days, causing a loss of about 1.7 billion dollars to airliners. Although no significant damage to aircraft was reported for this eruption, over 120 aircraft encounters with volcanic ash have nevertheless been documented between 1973 and 2008 (Schneider, 2009). The tracking of large ash clouds has therefore become a main concern in the last decades, as attested by the creation of Volcanic Ash Advisory Centers (VAAC) to provide their expertise to civil aviation in case of significant volcanic eruptions. Volcanic ash transport and dispersion (VATD) models are used to forecast the location and movement of ash clouds over hours to days in order to define hazards to aircraft and to communities downwind. Inputs are eruption source parameters such as plume height, mass eruption rate, duration, and mass fraction of fine ash (Mastin et al., 2009). Values of such parameters are frequently unconstrained in the first minutes or hours after an eruption is detected, and also change during an eruption (e.g. plume height), requiring rapid reevaluation. Dispersion model forecast are routinely validated, verified against all available observations, including field observations, combination of tephra deposits analysis and theoretical models, or in-situ measurements and sampling (aircraft). However remotely-sensed measurements by satellite imagery, ground-based radars and lidars, or better a combination of all, are the most efficient tools for real-time response owing to their continuous data acquisition and potential for automatic processing and rapid parameter quantification (Fig. 1).

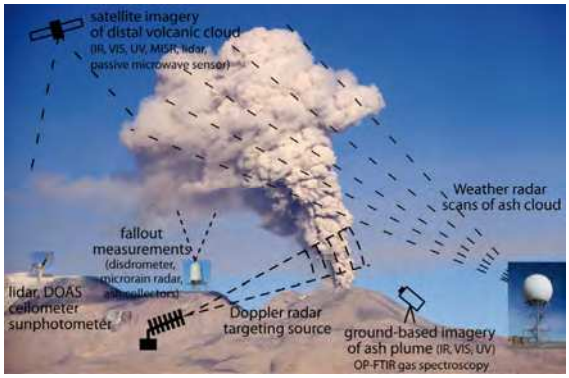

Fig. 1. Synergetic potential of integrated remote-sensing techniques for ash plume monitoring. Photo: Sabancaya volcano, courtesy of J.-L. Le Pennec.

2.2 Ash plume monitoring

Long-range trajectory tracking of ash clouds is achieved primarily by means of satellite imagery. Although Delene et al. (1996) showed the utility of a satellite-based microwave imager passively measuring radiations (19-85 GHz) of millimetric volcanic particles from an ash cloud of Mount Spurr in 1992, satellite visible-infrared radiometric observations from geostationary platforms are usually exploited (e.g., Rose et al., 2000). The evolution of the ash cloud spatial distribution, in particular, can be imaged at intervals of 15-30 min. Important parameters can be further retrieved like the approximate plume height assuming thermal equilibrium with the atmosphere (non unicity of solutions for altitudes above the tropopause), and the concentration and size of distal particles (< 20 microns) transported in the atmosphere, assuming particle sphericity and vertically homogeneous concentration. Using these assumptions, the mass of SO_2 and ash can be integrated on successive images (e.g. Wen & Rose, 1994). Scollo et al. (2010) also showed the potential of Multiangle Imaging SpectroRadiometer (MISR) working in four wavelengths in visible and near-infrared bands, for the 3-D reconstruction of ash plume shape, and for the retrieval of column height, optical depth, type and shape of the finest particles, among the most sensitive inputs for ash dispersal modeling.

Yet, the exploitation of satellite images for monitoring purposes is limited by (1) the presence of clouds at higher levels, (2) an insufficient acquisition rate for event onset detection, (3) a relatively poor spatial resolution, (4) errors of the "split-window" method (brightness temperature difference) when the volcanic plume lies over a very cold surface or when the plume lies above a clear land surface at night where strong surface temperature and moisture inversions exist (Prata et al., 2001). In addition, low ash content and/or small ash plumes might not be clearly observed and near-source emissions are obscured by the emitted tephra. For these reasons, ground-based radar systems represent an optimal complementary solution for real-time monitoring of these phenomena, by providing higher spatial resolution and data acquisition rates, as well as the ability to make observations at night and under any weather conditions. Real-time monitoring of ash plumes is crucial, in particular for the initialization of dispersion models. In this respect, essential input parameters such as plume height, mass flux, and particle concentration can be assessed quantitatively from radar data and directly contribute to improve ash dispersion forecasts.

2.2.1 Radar monitoring of ash plumes

2.2.1.1 Weather radar observations

2.2.1.1.1 Characteristics and advantages

Although ash plume hazards to aviation safety raised concerns early on about the detection capacity of ash clouds by airborne radar (Musolf, 1994; Stone, 1994), most observations of large volcanic ash clouds have been opportunely carried out by fixed meteorological radars of national weather services. Weather radars operate at microwave frequencies from S band (7.5-15 cm wavelength, generally about 10 cm) up to C band (3.75-7 cm wavelength, commonly around 6 cm), X band (2.5-3.75 cm wavelength, commonly around 3 cm) and Ka band (0.75-1.11 cm wavelength, often around 1 cm). With peak powers up to 250 kW or even higher, they have sufficient sensitivity to detect volcanic ash clouds with small particle sizes. Pulsed systems ensure a relatively high spatial range resolution of a few hundreds of

meters. Reflector antennas provide half-power beam-widths of a few degrees. These systems usually scan in azimuth and elevation, within a few minutes, allowing the maximum plume height to be tracked through time, along with the spatial variations of its reflectivity. Most have a Doppler capability to measure radial wind velocity, that can be used to infer information on internal velocities of ash clouds and retrieve information on turbulence, which has seldom been used. New generation radars are dual-polarized, which may further help to discriminate ash from hydrometeors.

Powerful weather radars, operating continuously at minute-scale acquisition rate and in all weather, have been used occasionally to track large ash clouds, chiefly since the first radar observations of Hekla eruption in 1970 and Augustine in 1976, because the information held in their records is many fold and potentially very useful for risk mitigation. Scan images of the ash cloud provide reflectivity variations in horizontal and vertical planes. Time evolutions of its height and lateral spreading can then be retrieved, along with its ascent rise rate and lateral transport speed. Mass and volume of radar-detected ash, as well as particle concentrations in the cloud can be estimated provided the grain size distribution can be constrained (from ash fall or other).

2.2.1.1.2 Observations

Harris et al. (1981), Harris & Rose (1983) and Rose & Kostinski (1994) first collected observations of ash plumes from Mt. St. Helens in 1980-1982 using 5 cm and 23 cm radar systems. They tracked the position of the ash cloud of March 19 1982, and estimated its volume (2000 ±500 km^3), the concentration of ash (0.2-0.6 g/m^3), reflectivity factors of 4-5 mm^6/m^3 (6-7 dBZ), and the total mass of ash erupted (3-10×10^8 kg). For the famous paroxysmal eruption of May 18 1980, they obtained a mass of 5×10^{11} kg, an ash volume of 0.2 km^3, and particle concentration of 3-9 g/m^3, for the ash cloud downwind of Mount St. Helens, 1.5-2 h after its eruption (horizontal speed 135 km/h). Reflectivity factors found for these dense (but distal) ash clouds (7-60 mm^6/m^3 or 8-18 dBZ) are several orders of magnitude smaller than those for severe weather considered routinely detectable by airborne weather radar and dangerous for aviation. Eruption-column rise rates and horizontal drift of ash clouds of Mount Pinatubo, Philippines, in 1991, were also tracked using two military C-band weather radars 40 km away (Oswalt et al., 1996). During the second eruption of June 12, 1991, radars indicated an apparent column rise rate in excess of 400 m/s. Radar height measurements were typically 10 to 15 percent lower than ash cloud heights inferred from satellite temperature analyses. Radar observations also suggested that higher eruption columns correlated with greater particle size and density within the column. Using a C-band radar Rose et al. (1995) found that most intense reflections in an ash cloud of Mount Spurr in 1992 came from particles 2 to 20 mm in diameter and with a total particle mass concentration of <0.01 to 1 g/m^3. The radar did not detect distal parts of the ash cloud, which have an atmospheric residence time of longer than 30 minutes, because the larger more reflective ash particles drop out. Maki and Doviak (2001) observed ash plumes of Mount Oyama on Miyake Island, Japan, in 2000, with a 5-cm (C band) radar, and proposed a method to obtain the time-dependent size distribution of ash particles from the time dependence of the reflectivity factor. Lacasse et al. (2004) reported observations of the ash cloud of the Icelandic Hekla volcano in 2000 with a C-band radar at Keflavík international airport. Reflectivity factors in the range 30 to >60 dBZ characterized the eruption column above the vent due to the dominant influence of lapilli and ash (tephra) on

the overall reflected signal, whereas values of between 0 and 30 dBz characterized the cloud advected downwind. The plume head had a mean ascent rate of 30 to 50 m/s up to 12 km in altitude (upper limit of the radar). Using the same radar, Marzano et al. (2006a, 2010a) found maximum reflectivities of 34 dBZ for the 2004 ash cloud of Grímsvötn volcano (260 km away), at a height of 6 km (minimum detection altitude). From an inversion technique based on a classification scheme of particles, they estimated ash concentrations of up to 6 g/m^3, and ashfall rates of up to 31 kg/h. Likewise, for the 2010 Eyjafjöll eruption, Marzano et al. (2011) determined an ash mass of up to 15×10^8 kg on April 16, and 8×10^7 kg on May 5. Recently, Marzano et al. (2010b) used volume scan data acquired in the S-band by a NEXRAD WSR-88D ground-based weather radar at Augustine vocano in Alaska in 2006 (Wood et al., 2007). From their model-based technique, ash aggregate concentrations of up to $0.2g/m^3$ were found to correspond to measured reflectivities of up to 55 dBZ at an ash column height of about 4 km. Maki et al. (2001) first reported observations of ash plumes from Mount Oyama in Japan by a 3-cm wavelength polarimetric mobile radar about 40 km away. They discussed the possibility of detecting volcanic ash particles and estimating their size distribution from polarimetric radar parameters such as the differential reflectivity and specific differential phase shift.

2.2.1.1.3 Limitations

As seen previously, ground-based weather radar systems are powerful tools for volcanic ash cloud detection and quantification. Their Doppler capacity has not, so far, been much exploited in the study of ash clouds and could aid understanding of the interplay between their dynamics and their environmental conditions (wind, atmospheric properties such as humidity and temperature profiles, etc). Their main limitations are, in general: (i) their limited sensitivity tending to render invisible to the radar the cloud parts where particle concentration is too low (ultimately all of the ash cloud). This leads to an underestimation of the ash cloud lateral extension, and also of its height because the top of the ash column may be coarse-depleted. Another source of error on column heights, and hence an underestimation of height-derived eruption rates, may come from the incomplete filling of the highest volume scanned by the plume top. The sensitivity of the ground-based radar measurements will decrease as the ash cloud moves farther away. (ii) By using single-polarization weather radar, however, it is fairly difficult to discriminate between ash, hydrometeors, and mixed particles. Ice nucleation and subsequent loss in reflectivity also make ash detection more difficult (Marzano et al., 2006b). These authors suggest that polarimetric radars may improve discrimination of the impact of cloud ice and liquid water on ash aggregates. According to Hannesen and Weipert (2011), however, significant overlap exists between meteorological targets and volcanic ash, so that, even if all polarimetric observables of dual-polarized radars are used, automatic detection might be tricky. With polarimetric data, however, the retrieval of volcanic parameters could be improved by taking into account the mixed particle composition and their shape (Marzano et al., 2012). (iii) Path attenuation effects are not always negligible. According to Marzano and Ferrauto (2003), in the case of hydrometeors, any radar technique above S band should take into account, and possibly remove, path attenuation effects in order to correctly convert measured reflectivity into rain rate. For ash clouds, Marzano et al. (2006b) concluded that C-band may offer some advantages in terms of radar reflectivity response and negligibility of path attenuation. While still tolerable at X-band, the path attenuation cannot be handled at

Ka-band. The advantage of higher frequencies (X-, Ka-band) is the potential diminution of the overall size of the system and a higher sensitivity to fine particles, hence a better detection at low ash concentration. For near-source soundings, path attenuation effects are presumably very important up to X-band and possibly non negligible up to L-band because of the high particle concentrations and sizes (commonly pluri-decimetric), especially in the gas thrust region. Further investigations are needed, even at L-band. (iv) Weather radars cannot track ash clouds over the long-term, due to the low atmospheric residence time of reflective coarse particles. (v) Their maximum detection range is generally within 200-300 kilometers of their fixed location. Portable radar systems overcome the limitation of observing ash clouds from a far distance and always the same volcano. In many respects, the synergetic role of satellite imagery in tracking volcanic ash, particularly after the initial stages of an eruptive event is obvious. (vi) Weather radars are unable to image the lowest few kilometers of the ash column when the volcano is too far away (and the top if above the beam), preventing early detection and retrieval of the near-source ash plume characteristics. To avoid some of these shortcomings, institutes in charge of volcano monitoring have started to integrate nearby dedicated radars into their instrumental networks.

2.2.1.2 Radars dedicated to volcano monitoring

Given the benefits of continuous quantitative retrieval of parameters such as height and mass loading which are crucial to initiate dispersion models, permanent volcano monitoring using weather radars has become more widely used. Ground-based weather radar networks are currently operational at several volcanoes, in Alaska, Iceland, Italy and Guadeloupe. The U.S. Geological Survey first experimented in 1997 with a ground-based Doppler radar at the National Center for the Prevention of Disasters (CENAPRED) in Mexico to track the dispersal of ash plumes of Popocatépetl volcano and at least two eruptions were successfully captured. In addition to the near contiguous network of weather-monitoring Doppler radar NEXRAD operated by the U.S. National Weather Service, the U.S. Geological Survey also deployed a new truck-transportable C-band Doppler radar (MiniMax-250C) during the 2009 eruptions of Redoubt Volcano, Alaska (Hoblitt and Schneider, 2009). Results for 17 ash plumes detected by the radar compared favorably well with those of a nearby WSR-88D NEXRAD operated by the Federal Aviation Administration. The sector-scanning strategy (45°) of the new mobile radar advantageously allowed event onset detection within less than a minute. Heights (9-19 km) and vertical rise rates of the ash columns (25-60 m/s) have been determined. The high radar reflectivity values of the central core of the eruption column (50-60 dBZ) were interpreted as being the result of rapid formation of volcanic ash-ice aggregates (Schneider, 2012).

The X-band is generally preferable providing higher sensitivity with respect to lower frequency bands typically used for weather observations. The Japanese government recently set up an X-band polarimetric radar near Sakurajima volcano, able to monitor its recurrent vulcanian ash plumes (M. Maki, pers. comm.). Since November 2010, the Icelandic Met Office has had on loan from the Italian Civil Protection a mobile X-band dual-polarization radar for volcano monitoring. This radar (75 km from the volcano), along with the fixed weather C-band radar in Keflavík (257 km from the volcano), monitored the ash plumes of Eyjafjoll in 2010 and Grimsvötn in 2011 (Arason et al., 2011, 2012). These authors used in particular the radar time-series of the plume heights to calculate the mean eruptive flow

rate. From the polarimetric X-band dataset of this eruption, Hannesen and Weipert (2011) quantified ash concentrations of up to 100 g/m^3 and ash fall rates of up to 100 kg/m^2/h at a height of 4.5 km from all polarimetric observables. They emphasize, however, the limits of ash quantification, the ambiguity in the separation of precipitation and ash that makes automatic detection still difficult, and the signal weakness from distant ash that prevents radar observations. Vulpiani et al. (2011) explored the benefits of the mobile dual polarization X band radar (DPX 4) operated by the Department of Civil Protection at the airport of Catania Fontanarossa (30 km to the South) to monitor Etna and offer support to the decisions of the authorities that regulate and control air traffic. In an ash plume fed from a lava fountain, maximum reflectivities of 35 dBZ were measured at medium distances of 10-40 km from the volcano. Estimated mass concentrations vary up to a few g/m^3, although most are below 1 g/m^3. The instrumental monitoring network of Etna operated by the Istituto Nazionale di Geofisica I Vulcanologia (INGV) also comprises, since 2009, and this is unique, a permanent ground-based L-band Doppler radar of the Observatoire de Physique du Globe de Clermont-Ferrand (OPGC, France) targeting the summit craters (Donnadieu et al., 2009a, 2012). Named VOLDORAD 2B, this radar is similar to the transportable volcano Doppler radar (VOLDORAD) successfully applied in several volcanic contexts (Dubosclard et al., 1999, 2004; Donnadieu et al., 2003, 2005), as illustrated later in this chapter (cf. section 7.1, fig. 16). The permanent radar at Etna should complement observations from the INGV monitoring network to constrain the inputs of the tephra dispersal models run automatically to perform tephra dispersal forecast (Scollo et al., 2009).

2.2.1.3 Fallout measurements

A compact X-band continuous wave, low power (10 mW) Doppler Radar (PLUDIX, 9.5 GHz frequency of operation), originally designed as a rain gauge disdrometer, was utilized to measure the terminal settling velocities and infer sizes of plume fallout at Mount Etna in 2002 (Scollo et al., 2005) and Eyjafjallajökull in 2010 (Bonadonna et al., 2011). PLUDIX-derived particle size distributions agree reasonably well with sieve-derived grain size distributions, but only for diameter range above 500 microns, and so should be used within a few kilometers from the source. Such measurements, along with deposit sampling and other methods shown in figure 1, can usefully complement other radar observations of the ash plume/cloud (Fig. 1) by providing the particle size distribution necessary to accurately retrieve the loading parameters (total mass, mass concentrations, mass flux of tephra).

2.2.1.4 Compact portable Doppler radars for near-source measurements

The growing need to get insight into the dynamics of explosive eruptions and to measure eruptive parameters at the source has led to the development of several active remote sensing compact instruments in the last decade or so. The first attempt to bring transportable sounders close to volcanic craters to measure the near-source dynamics was achieved by Weill *et al.* (1992) who successfully determined vertical velocities in the range 20-80 m/s for over 100 mild Strombolian explosions at Stromboli using a Doppler sodar. This cumbersome acoustic sounder could operate only at a few hundred meters from the vent and, hence, was not well suited to the sounding of larger magnitude, hazardous eruptions. Besides, velocity determinations using sodar require the knowledge of sound velocity at the jet temperature and gas composition, which was not available. Two main types of dedicated portable radars have since been used with the primary goal of studying

eruption near-source dynamics through their Doppler capability: commercial micro rain radars, that are continuous-wave frequency-modulated and working at 24 GHz (Seyfried & Hort, 1999; Hort et al., 2003, 2006) and the VOLDORAD system, an L-band pulsed volcano Doppler radar (e.g., Dubosclard et al., 1999, 2004; Donnadieu et al., 2005). Being set up at a chosen location and aiming directly at the emission source (instead of rotation scanning), these compact radar systems can advantageously sound the gas thrust region and provide source eruptive parameters like eruption velocities, but also capture short-lived weak explosive activity, not visible to satellites or weather radars. They have higher temporal (<1 s) and spatial resolutions (tens to hundreds of meters) and higher sensitivity. A comparison of some characteristics of weather radars and transportable volcano Doppler radars is presented in Table 1.

	Location	Max. range	Min. range	Acquisition rate	Volume scanned	Power consumption	Frequency bands
Weather radars	Fixed	100-300 km	Few km	Few min	km^3	100s of kW	S, C, X, Ka
Portable radars	Chosen	10-15 km	10s-100s m	≤ 1 s	10^4-10^8 m^3	Few mW to few 10s of W	L, X, Ka

Table 1. Characteristics of weather and transportable radars for the monitoring of volcanic eruptions. Note in particular the difference in temporal and spatial resolution.

Hort and Seyfried (1998) and Seyfried and Hort (1999) measured mean vertical velocities of about 10 m/s for 12 lava jets during very low activity at Stromboli volcano with a commercial portable FM-CW radar Doppler anemometer 200-300 m away from the eruptive vent. Using the same instrument, Hort et al. (2003) found an increase in eruption duration, much higher velocities and indirect evidence of mean particle size decrease after a rain storm. Gerst et al. (2008) reconstructed the 4D velocity (directivity) of Strombolian eruptions at Erebus and Stromboli from 3 FM-CW radars. FM-CW radars have a narrower field of view (around 1° or so at 3 dB) and can thus target a precise sector of the volcanic emission but, on the other hand, lack the integrated information of longer wavelength pulse radars with a wider beam aperture and deeper range gates. L-band frequency signals are very little attenuated by hydrometeors or volcanic particles and can sound the interior of very dense particle-laden plumes. VOLDORAD also has a higher temporal resolution (<0.1 s).

Donnadieu et al. (2005) showed very detailed time series of power and maximum radial velocities of a Strombolian explosion at Etna and an ash plume at Arenal, acquired at high rate (<0.1 s) with VOLDORAD. Donnadieu et al. (2003, 2005) and Dubosclard et al. (2004) further showed evidence of strong correlation between volcanic tremor and maximum radar velocities for several Strombolian episodes, suggesting the influence of gas bubble dynamics in the conduit on tremor generation at Etna. Using VOLDORAD, Gouhier & Donnadieu (2008) first quantified the mass of tephra of Strombolian explosions at Etna (50-200 tons) from a new power inversion method. From the analysis of the shape of Doppler spectra of 200 Strombolian explosions, Gouhier & Donnadieu (2010) found that 80% of the load is ejected within a 40° dispersion cone and that, for 2/3 of the explosions, ejecta are distributed uniformly within this cone. Using measured maximum radial velocities, at-vent particle and gas velocities can be retrieved, and source gas fluxes estimated when the vent diameter is known (Gouhier & Donnadieu, 2011). Comparing thermal data with records from a FM-CW

at Stromboli, Scharff et al. (2008) found a correlation between the radiative energy of Strombolian lava jets and the backscattered energy, suggesting that both methods record the relative variations of mass. They also found pulsations in the power time series of 40% of the eruptions, likely reflecting variations in mass eruption rate and originating in multiple consecutively exploding bubbles.

Scharff et al. (2012) also report the pulsed release (2-5 s) of ash clouds from the dome of Santiaguito with particle radial velocities between 10 and 25 m/s, and preceded by a vertical dome uplift of about 50 cm, as recorded with a FM-CW radar. Using VOLDORAD, Donnadieu et al. (2008) had already reported staccato pressure release in the ash emissions of Arenal volcano, along with a variety of ash plume dynamics from short-lived explosive events with radial velocities of up to 90 m/s, to sustained pulsed ash jetting and to passive dilute ash emissions. Donnadieu et al. (2011) successfully reconstructed the 3D vector of the ash plume transport speed from the echo onsets in contiguous range gates.

3. Specificity of radar signals of volcanic origin

3.1 Examples of meteorological signals

While abundant literature describes the effects of meteorological targets on weather radar signals, few studies characterize volcanic targets from a radar perspective. Not only the dynamics of volcanic eruptions strongly differs from that of common meteorological phenomena but also the target properties. This section points out some differences relevant to the study of radar signals of volcanic origin, for measurements near the emission source and in the distal part of ash clouds.

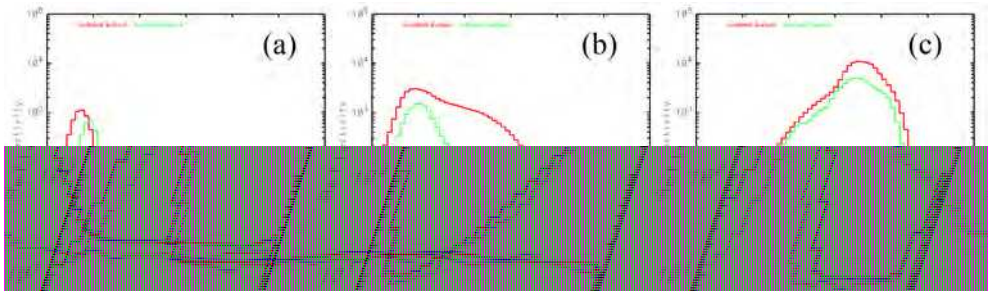

Fig. 2. Examples of meteorological Doppler spectra from a 24 GHz Micro Rain Radar. Reflectivity is shown versus radial velocity (i.e. fall speed with vertical beam) at a 1 hour interval (6:05 U.T. in red and 07:05 U.T. in green) on 21/12/2011: (a) snow crystals at 1430-1730 m a.s.l., (b) mixture of melting snow and water droplets in the radar bright-band (930-1230 m a.s.l.), (c) melt water droplets at 430-730 m a.s.l.. Data of MRR4 at Aulnat Airport (France): courtesy of Yves Pointin (OPGC).

Typical Doppler spectra of meteorological targets showing reflectivity versus fall speeds are presented in figure 2. Because the sounding is vertical, radial velocities (toward the radar) directly indicate fall speeds, unlike in the oblique radar soundings of volcanic emissions. At altitude, low reflectivity snow crystals fall at low speed (Gaussian shape spectrum). At intermediary altitude, a mixture of melting snow and water droplets (radar bright-band)

produces more complex spectrum shapes, whereas at lower altitude melt water droplets produce rainfall with high reflectivity (Z>40 dBZ) and higher fall speeds up to 10 m/s. Note the relatively low velocities and spectrum width, as compared with the volcanic emission recorded by VOLDORAD (right panel in figure 3).

3.2 Volcanic features relevant to radar investigations

The contrasted radar signatures from meteorological targets and volcanic emissions are particularly conspicuous in figure 3 showing Doppler spectra recorded by VOLDORAD for rainfall and at the base of a weak ash plume during an explosive event. Whereas the rainfall shows narrow power distribution with a similar weak intensity and a well defined mode at 12 m/s over many range gates, volcanic tephra backscatter much more power spread over a radial velocity range from -30 to +60 m/s in just the two range gates above the eruptive vent.

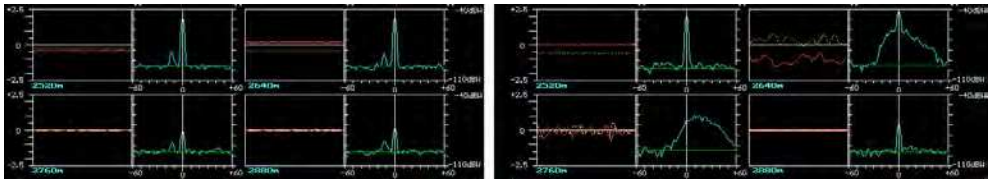

Fig. 3. Doppler spectra recorded by VOLDORAD for rainfall and tephra emission. The snapshots show the signals and power spectral density recorded in 4 range bins (120 m deep) between 2520 and 2880m on 18 February 2004, with a beam elevation angle of 27°. Central ground clutters are not filtered. *Left*: rainfall; *right*: ash plume event.

In addition to the sounding geometry effect, the large contrasts in echo power and velocity distribution (spectrum shape) observed in signals of volcanic origin relative to meteorological ones come at first order from the target sizes, velocity field, trajectories, with huge variations of these in amplitude in time and space, especially near the volcanic source.

The sizes of tephra currently range from decimetric or even metric to micronic particles (6 orders of magnitude) close to the vent while only particles microns to tens of microns in diameter can remain in the atmosphere for days. While Strombolian eruptions consist of the recurrent ejection of small-medium volumes of incandescent lava bombs and lapilli with commonly minor amounts of ash to heights of tens to hundreds of meters, the fragmentation of lava and particle dispersion are much higher in eruptions generating ash plumes. From a radar perspective, the backscattered power is strongly controlled by the larger particles. Consider for instance that an order of magnitude change in particle size leads to an increase by a factor of 10^6 in the reflectivity factor in the Rayleigh domain. However, the relative proportions of each size also counts, so the particle size distribution is of primary importance, albeit challenging to measure accurately over the full size range. Importantly, particles exceeding several centimeters (lapilli and blocks) present in most volcanic tephra emissions, prevent the use of the Rayleigh approximation to quantify near-source products and the Mie formulation must be used at all infra-metric wavelengths.

Because volcanic emissions are made up of a mixture of hot gases, lava and solid fragments of various sizes ejected at high speed (tens to hundreds of m/s) from a vent, their dynamics

is complex and rapidly varying in time and space. The moments and shapes of Doppler spectra also fluctuate rapidly, with spatial variations among the range gates related to the dimension of the phenomenon with respect to the sounded volumes. The power spectral density results in particular from the complex combination of the particle velocity field and particle load distribution, i.e. the amount of particles, their velocities and trajectories. Being either short-lived or sustained, volcanic emissions can be roughly viewed as two-phase flows generally oriented vertically upward with a continuum of dynamic behaviors from inertial large blocks mostly following ballistic trajectories soon after their ejection down to the finest low-inertia particles nearly following the gas behavior involving a stronger deceleration soon after their emission. Crosswinds also affect the particles' motion differentially according to their diameter and residual momentum. Gravity further implies that ejecta are propelled upward while others fall out simultaneously and both imprint their signature in near-source radar measurements.

Volcanic emissions are generally highly turbulent close to the source (gas thrust region and convective part) and less turbulent in the distal cloud. The effect of turbulence in the cloud is difficult to assess because the particle behavior is highly size-dependent, from inertial large blocks to gas-entrained fine particles. Although assumed not to be dominant in radar measurements near the source where large particles are present, the turbulence effects affecting overall the small particles should nevertheless tend to increase the spectral width, as observed in radar meteorology.

3.3 Target properties

At second order, the intrinsic properties of the targets, their movements and chemico-physical evolution, also play a role in the measured reflectivity. Because volcanic tephra generally originate from the violent fragmentation of magma by the expanding gas, their shape is also complex and their surface highly irregular at various scales. The effects of shape and roughness of volcanic particles on reflectivity have been little investigated at radar wavelengths. Yet they might be non negligible, at least at short wavelength, as suggested for meteorological targets. In examining the effects of ice crystal shapes on reflectivity at 3 mm wavelength, Okamato (2002) found, for instance, 8 and 5 dB effects of non-sphericity and orientation respectively, for particle sizes approaching the wavelength. In the volcanic case, the analysis is further complicated by in-flight modifications of the ejecta shape and orientation, especially close to the source. Large lava fragments, in particular, deform in-flight due to their plastic nature, as attested by the specific shapes of volcanic bombs (e.g. fusiform), or break up upon impact with other ejecta and because of high strain rates imposed by acceleration, rotation, and drag force. It must be expected that most fragments have a rapidly changing orientation in flight, especially close to the source where turbulence occurs.

Water vapor being the dominant gas species exsolved from magma (commonly >85%), major condensation by the cold atmosphere occurs during eruptions. There is 2.4 factor difference between the dielectric factors of ash (0.39: Adams et al., 1996; Oguchi et al., 2009; Rogers et al., 2011) and liquid water (0.93). According to studies by Oguchi et al. (2009) from 3 to 13 GHz, a water film coating 10-20% of the radius of a sub-millimetric volcanic particle is sufficient to raise the radar cross section to that of a whole liquid water particle (0.93 dielectric factor). Water vapor further promotes the nucleation of ice (0.197 dielectric factor)

in ash plumes at high altitude, depending on the vertical atmospheric temperature profile, and favors aggregation of ash particles. Thus, ice formation has a double effect on reflectivity, acting both on the dielectric properties and the size (aggregation). Although the influence of temperature on the dielectric properties of rocks seems rather limited up to 900°K (Campbell & Ulrichs, 1969), possible effects of magmatic temperatures need to be checked. The decrease of rock permittivity with silica content observed by these authors has direct consequences in terms of radar retrievals from eruption products of different composition, from basaltic to dacitic or rhyolitic for instance. As the combined contributions of all these effects might significantly change the reflectivity of ash plumes, they need to be further characterized physically, along with the relevant volcanic particle characteristics, in order to improve the accuracy of volcanic retrievals from radar returns.

4. VOLDORAD, a dedicated volcanological Doppler radar

4.1 Description of the transportable radar

VOLDORAD is a ground-based pulse volcano Doppler radar specifically designed at the Observatoire de Physique du Globe de Clermont-Ferrand (OPGC) for the monitoring of the surface volcanic activity of variable intensity. It can be deployed rapidly near an eruptive vent and target the near-source activity to measure in real-time the eruptive velocities and backscattered power and give information about the amount and rate of tephra emission.

Fig. 4. (*left*): The transportable volcano Doppler radar VOLDORAD 2 deployed at Arenal. The PC and radar in the car trunk are connected to the antenna system via a switch box and fed by a small generator. *Upper inset*: Radar with PC for data storage and real-time monitoring and GPS receiver for time synchronization; *lower inset*: antenna (square array of Yagi) aiming at the summit to sound ash emissions. Photos: courtesy of S. Valade, OPGC (2009).

Fig. 5. (*right*): Principles of near-vent soundings with VOLDORAD.

The signal wavelength (23.5cm) was chosen (i) to sound the interior of dense lava jets and ash-laden plumes, as well as (ii) to avoid attenuation by hydrometeors because cloudy, foggy, rainy, or snowy conditions often occur at volcano summits. It also results from a compromise between transportability (weight, size), variable measurement distances (0.2-12 km) imposed by field conditions, and the HF hardware facilities available at the OPGC.

Acquisition, reception and pre-processing units are mounted on a suspended frame inside a protective metal container (60 cm, 50 kg). A PC controls the radar acquisition, being synchronized to UTC time through a GPS or ethernet connexion, and is used for real-time visualization of Doppler spectra and data storage. The 23 elements' square array antenna is mounted on a tripod adjustable for site and azimuth, and can be easily dismantled for transport. The 3 dB beam width is 9°, equivalent to site and azimuth resolutions of about 160 m at 1 km. The 300 W power consumption is provided through a small electric generator or AC. Owing to its modularity and limited weight (~70 kg), the ensemble is easily transportable, fits in a 4WD vehicle, and can be set up quickly in a volcanic environment. This radar can thus be used for short-term scientific campaigns, as well as over the long term for monitoring purposes.

A number of settings have been designed to be selectable to best adapt to the activity and the sounding conditions. The pulse duration is selectable from 0.4 to 1.5 μs so that the range bin radial resolution can be chosen between 60 and 225 m according to the target dimensions and the type of information searched for. The pulse repetition frequency can be 50, 100 or 200 μs. The non ambiguous maximum range at a 100 microsecond repetition frequency is 12 km. The gain attenuation can be varied by 50 dB through 10 dB steps to best adapt to the eruption intensity. The format of the data stored on the PC hard disk can be chosen in order to adjust the space memory consumption to the duration of the record campaign: either the time series of the raw digitized signal can be recorded, i.e. after coherent integrations in the time-domain, or alternatively only the spectra are saved, i.e. after integrations in the frequency domain.

4.2 Echoing mechanism

A powerful short radio frequency pulse (duration τ) is periodically transmitted into the atmosphere through a switch and a directive antenna which concentrates the energy in a narrow beam. Just after the pulse transmission, the switch connects the antenna to a radio frequency receiver. If targets are located in the antenna beam, part of the pulse energy is backscattered toward the antenna. These radar echoes are fed via a switch to the receiver for amplification and filtering. At the receiver output, the electromagnetic signal is detected and converted into digital data which are then processed and recorded.

Like in the case of atmospheric sounding, two main mechanisms give rise to radar echoes in the case of volcanic targets (Sauvageot, 1992; Doviak and Zrnic', 1993; Dubosclard et al., 1999): (i) Rayleigh ($D < \lambda/4$) or Mie scattering ($D \geq \lambda/4$) from distributed targets, and (ii) Bragg scattering from spatial irregularities of the refractive index induced by turbulent eddies inside the hot jet, and supposedly of secondary importance in the volcanic case because of the large reflectivity of tephra. In addition to the distance of the sounded volumes, the radar reflectivity (η) is deduced from the intensity of the echo signal by using the radar equation:

$$P_r = C_r \frac{\eta}{r^2} \tag{1}$$

where P_r is the echo power measured by the radar receiver and C_r a constant including the radar parameters such as transmitted power, pulse duration, wavelength, antenna

characteristics, gain or half power beamwidth. In the simplest case of Rayleigh scattering ($D < \lambda/4$), η is expressed as:

$$\eta = \frac{\pi^5}{\lambda^4} |K|^2 \, Z \tag{2}$$

where K is the complex dielectric constant of the targets ($|K|^2$ =0.39 for ash (Adams et al., 1996; Oguchi et al., 2009; Rogers et al., 2011) and Z the radar reflectivity factor. For spherical targets, Z is given by:

$$Z = \int_0^\infty N(D) D^6 \, dD \tag{3}$$

where $N(D)dD$ is the number of targets per unit volume whose diameters are between D and $D+dD$. Z is generally expressed in dBZ units, defined by:

$$Z(\text{dBZ}) = 10 Log\left[Z(\text{mm}^6.\text{m}^{-3}) \right] \tag{4}$$

For Mie scattering ($D \geq \lambda/4$), one generally uses the so-called equivalent radar reflectivity factor (Doviak and Zrnic', 1993), which is defined as the radar reflectivity factor of a small particle population satisfying the Rayleigh approximation and that would return the same received power. Interestingly, Z characterizes only the target and holds information on the number and size of particles, and thus on the particle concentration. The reflectivity factor obtained from radar measurements is usually calibrated using the dielectric factor of liquid water (0.93) and must be corrected for volcanic ash as the dielectric factor of the latter is lower (0.39):

$$Z_{ash} = \frac{|K|^2_{water}}{|K|^2_{ash}} Z_{water} = 2.38 Z_{water} \tag{5}$$

Finally, the radial velocity (V_r) of the target is calculated from the frequency shift between the transmitted and received signals. The velocity component along the antenna line of sight (toward or away from the radar) causes the returned frequency f_r to be different from the transmitted frequency f_t (Doppler effect), and is proportional to the Doppler shift f_d:

$$f_d = f_r - f_t = -\frac{2V_r}{c} f_t = -\frac{2V_r}{\lambda} \tag{6}$$

Note that a negative Doppler shift ($f_r < f_t$) corresponds to a target with a radial component of motion away from the antenna (positive radial velocity) and *vice versa*. Furthermore, if the velocity vector is normal to the antenna direction, the Doppler shift is zero. In volcanic soundings, the antenna beam can be set either to point upward, e.g. from the volcano slope toward the summit, or downward, for instance aiming toward the eruptive vent from the crater rim. In these cases, contributions of rising and falling particles to the spectra are reversed (Fig. 6).

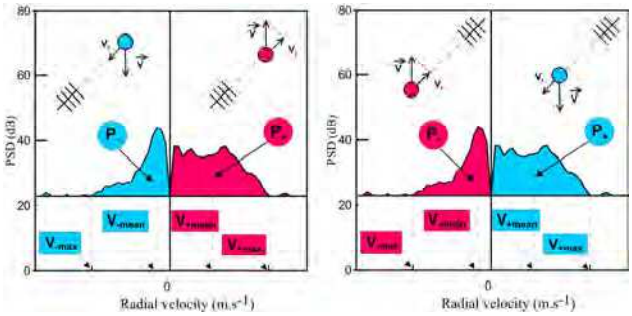

Fig. 6. Volcanic particle contributions to Doppler spectra in different sounding conditions. (a) When the antenna points upward (e.g. at summit craters from the flanks), ascending volcanic particles in red induce echoes with an along-beam velocity component away from the radar (positive radial velocity range, right part of spectrum), whereas falling particles in blue induce radial velocities toward the radar (negative radial velocity range, left part of spectrum). (b) The contributions are reversed when the antenna beam points downward (e.g. down towards a crater from the rim).

For a given range gate and for each component of the complex raw signals, N_c successive digitized samples (coherent integrations) are added together and then averaged in the time domain. This integration process acts as a low-pass filter reducing the high frequency noise and improving the signal-to-noise ratio. In order to avoid aliasing, the value of N_c must be adapted to expected maximum eruption velocities, in such a way that the Nyquist frequency f_N is higher that any Doppler frequency:

$$f_N = \frac{1}{2N_c T_r} \tag{7}$$

where T_r is the pulse repetition period of the radar. From (6) and (7) it results that the maximum radial velocity which can be measured without ambiguity is given by:

$$V_{\max} = \frac{\lambda}{4N_c T_r} \tag{8}$$

After N_c pulses have been integrated, the coherent integration stage is repeated until a sequence of 64 integrated complex data is obtained. For each range gate, the 64 coherently integrated complex data are used as a time series input to a FFT (Fast Fourier Transform) algorithm in order to obtain the power spectrum of the radar echo. The frequency resolution (frequency interval between two consecutive spectral lines) is given by:

$$\Delta f = \frac{1}{64\, N_c\, T_r} \tag{9}$$

Therefore, the corresponding velocity resolution is:

$$\Delta V = \frac{\lambda}{128\, N_c\, T_r} \tag{10}$$

A mean spectrum can be finally calculated from the averaging in the frequency domain of several consecutive spectra (incoherent integrations) to reduce the noise fluctuations in the resulting Doppler spectra and improve the detection of the spectral line(s) corresponding to the volcanic echoes.

5. Insight into the dynamics of Strombolian activity

In addition to measuring eruptive parameters near the emission source, the main advantage of portable Doppler radars with respect to weather radars resides in the fact that they can be set up close to an eruptive vent and target just one direction at the base of the volcanic flow to retrieve near-source parameters. They are thus able to monitor phenomena of limited spatial dimensions with better spatial resolution and higher acquisition rate. In this respect, they are particularly useful for studying Strombolian activity and small scale ash plumes, generally invisible to remote weather radars and satellites. Although VOLDORAD can also be used to monitor strong ash-laden plumes, given its wavelength, examples of records on such types of activity are provided respectively in this section and the next.

5.1 Information retrieved from the shape of Doppler spectra

5.1.1 Ejecta dispersion

Given the relatively low amount of ash produced during typical Strombolian activity, the echo power is mostly controlled by large blocks that mostly follow ballistic trajectories. An illustration of the strong control of the ejecta's spatial distribution on the shape of Doppler spectra is the discrimination between lava bubble outbursts and lava jets (Fig. 7). When the magma column is high in the conduit, large gas bubbles may deform the lava surface to form lava bubbles several tens of meters in diameter, whose outburst disrupts the surrounding lava film and produces the hemispherical ejection of big lava lumps (decimetric to metric) seen above the crater rim (Fig. 7a). Contrastingly, in the vast majority of events, gas slug explosions occur within the conduit and produce oriented jets of gas and more fragmented lava, generally vertical, that can be captured by the radar beam when (if) pyroclasts go beyond the crater rim (Fig. 7c). Velocity and mass load angular distributions of pyroclasts are, as expected, more uniform for hemispherical lava bubbles that can burst at the free surface and more Gaussian-shaped for lava jets that are subjected to conduit wall friction (Fig. 8). In the case of hemispheric lava bubbles, the uniform mass load and velocity distribution of pyroclasts over the range of ejection angles produce an equal echo power over the range of radial velocities, leading to top-hat shaped spectra (Fig. 7b). In the case of lava jets, the power spectral distribution results from the competing effects of particle velocities and the distribution of ejection angles. As shown in figure 8b, measured maximum radial velocities do not result from particles with the highest velocities in the jet axis, nor from those having the most radial trajectories, but from particles ejected at about 20° to the jet axis (when vertical). Therefore Doppler spectra commonly appear rather triangular when shown in dB (Fig. 7d). Gouhier & Donnadieu (2010) found that, for most Strombolians explosions at Etna, 80% of the tephra mass is ejected within a dispersion cone of about 40°.

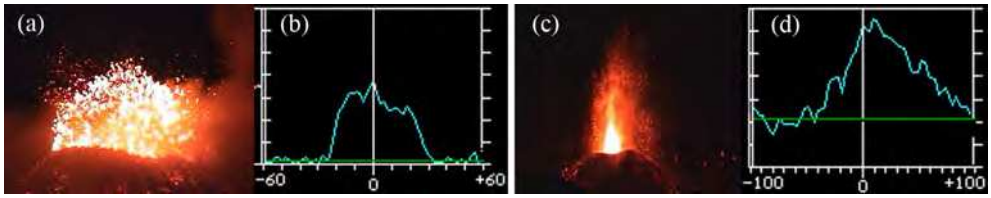

Fig. 7. Shapes of Doppler spectra associated with Strombolian activity. Outburst of a hemispherical lava bubble (a) and associated top-hat Doppler spectrum (b) at Etna's SE Crater (04/07/2001, 21:43'06). (c) Vertical lava jet at Laghetto (29/07/2001, 21:20'56) and the recorded triangular spectrum (d) (power in dBW vs. radial velocity in m/s).

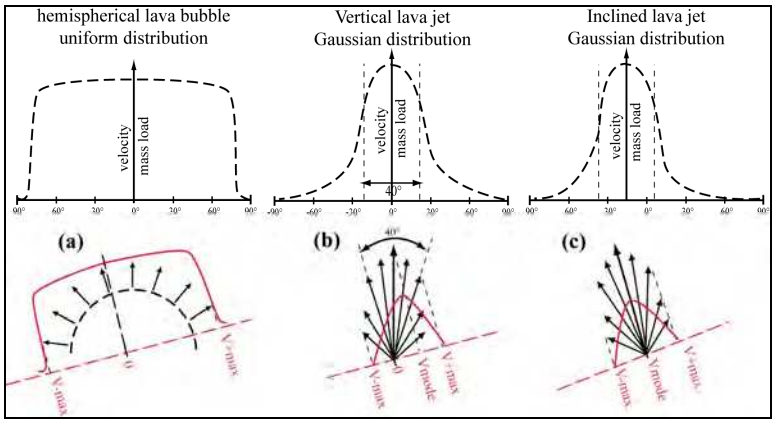

Fig. 8. Ejecta angular distributions (*top*) for lava bubbles (a), vertical jets (b) and inclined jets (c) and associated characteristics of Doppler spectra in red (*bottom*). (a): similar to Fig. 7a & 7b; (b): similar to Fig. 7c & 7d; (c): case of a jet inclined toward the radar.

All intermediary types of pyroclast ejection may exist, including lava jets with low directivity, leading to varied spectrum shapes. The latter can be further complicated by other factors related to the lava state in the conduit and crater, or to gas slug characteristics (overpressure, length) that may enhance fragmentation and produce more fine particles more closely coupled to the gas dynamics.

5.1.2 Inclination of lava jets

Strombolian activity is often imagined as an axi-symmetric dispersion of ejecta around the vertical, but departures are frequently observed from one explosion to another, and ejection in a preferential direction may even persist if conduit conditions are favorable. Relative variations of the ejecta dispersion axis from the vertical, i.e. the inclination of lava jets or lava bubble outburst, can be tracked from the mode of the radial velocities, i.e. the velocity associated with the maximum power in the main range gate (Fig. 8b,c). The velocity mode is shifted toward the maximum negative radial velocities (aiming upward) when the lava jet has an inclination component toward the radar (Fig. 8c) and vice versa. The power distribution in contiguous gates also puts constraints on the ejection geometry and

velocities. In figure 9, for instance, ejecta emitted below the 840 m range bin do not reach the 600 m range bin, falling ejecta reaching the 720 m and 960 m bins where the negative parts of the spectra look alike. The absolute inclination angle cannot be retrieved directly firstly because velocities and power distribution vary strongly between explosions and also only the inclination angular component in the beam's vertical plane can be retrieved. Gerst et al. (2008) solved this problem by using simultaneously 3 FM-CW radars to calculate the directivity of Strombolian eruptions and reconstruct time series of the 3-D directivity vector every second. Another solution is to best match the power spectral distribution in the different range gates (e.g., Fig. 9) from ballistic models and Mie scattering theory (Gouhier & Donnadieu, 2010).

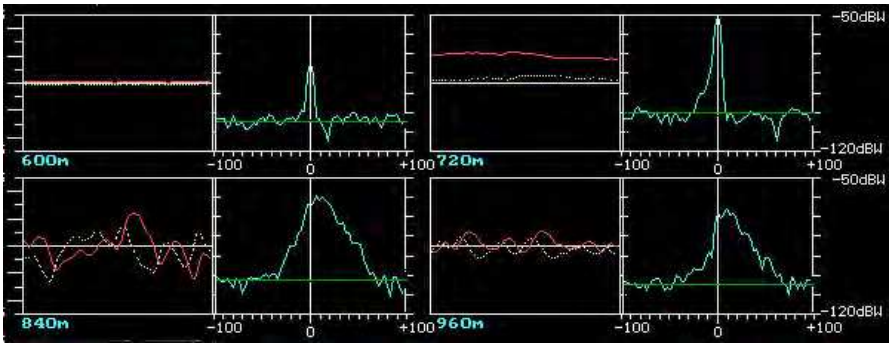

Fig. 9. Doppler spectra recorded in 4 range bins during lava jet activity at Etna. For each gate the raw signals (left) and spectra (right) seen in real-time are shown. The spatial distribution of the power spectral density in the 840 m range gate above the eruptive crater and in contiguous range gates (720 and 960 m) gives information about the dynamics of the lava jets (Laghetto cone, 29/07/2001).

5.2 Information from spectral moments

5.2.1 Mean diameter

Dubosclard et al. (2004) have shown that, in the case of Strombolian activity, the negative power spectral density (when aiming upward) of the range gates above the vent is mostly associated with falling particles. Therefore, the mean negative radial velocity weighted by the power spectral density has been used to retrieve the average particle diameter in the jet, commonly found to be between 1 and a few cm in diameter. Importantly, Gouhier & Donnadieu (2008) pointed out that the radar-equivalent mean diameter retrieved from Doppler spectra differs significantly from the true mode of the particle size distribution which, indeed, corresponds to the most frequent diameter encountered. Thus the radar-equivalent mean diameter cannot be used directly as the true modal diameter. In the gas thrust region of volcanic jets, the power spectrum is very wide, unlike in radar meteorology, and the physical interpretation of the radar-equivalent mean diameter is complex. Because the offset factor depends upon the reflectivity at a given radar wavelength, itself dependent on the number and diameter of particles which vary over a wide range, the conversion requires the Mie scattering formulation.

5.2.2 Eruptive velocities

Initial velocities are of great interest because they control the height reached by the pyroclasts and are related to the gas overpressure. In measuring particle velocities continuously and at high rate, Doppler radars potentially hold information on these parameters and on the detailed kinetics of the jets. Although the variations of measured radial velocities closely reflect the kinetics of the volcanic jet, retrieving absolute initial particle velocities from measured maximum radial velocities is not straightforward, in general, because (i) the latter are associated with oblique trajectories, as illustrated in figure 8b-c, (ii) the distance between the range gate's lower boundary and the emission source must be taken into account; it also controls which particle size induces the measured maximum velocities (Gouhier & Donnadieu, 2011). In order to confidently retrieve initial (at-vent) velocities, eruption models with suitable laws are needed, along with accurate knowledge of the sounding geometry and crater configuration. Velocity calibration can be further supported by an analysis of video-derived velocities. By sounding the volcanic emission near their source, it turns out often that maximum radial velocities, commonly in the range of a few tens to 160 m/s are not very different from eruptive velocities during Strombolian activity at Etna for example. Gouhier & Donnadieu (2011) analyzed 247 Strombolian explosions during the paroxysmal phase of the July 4 2001 eruptive episode of Etna's SE crater and found time-averaged values of 95 ±24 m/s for initial particle velocities, 37.6 ±1.9 m/s for the bulk jet velocity, and 118 ±36 m/s for the initial gas velocity. Note that the initial gas velocity is highly dependent upon the chosen model law, as the gas velocity decrease with height is exponential and more quantitative observations are needed, using complementary techniques like high-rate thermal infrared imagery.

5.2.3 Detailed dynamics at short time scales

Much can be learned from the analysis of time series of echo power and velocities on the eruption dynamics at various time scales, ranging from a single explosion through to an entire eruptive episode, to a series of eruptions. Figure 10 shows such time series for a Strombolian explosion at Yasur volcano, Vanuatu, similar to that shown in figure 11.

The maximum along-beam velocities associated with rising ejecta show a very sharp increase up to a peak near 120 m/s within 0.21 s, attesting to initial accelerations of over 560 m/s^2 (i.e. 57 g). Measured velocities then regularly decrease for 6-7 s, then reach a plateau at 20-30 m/s with sparse, short fluctuations up to 50 m/s. Interestingly, during the strong velocity phase, ample fluctuations associated with short power increases can be seen pulsating every ~1.5 s, suggesting rapid variations in the discharge rate. This could be caused either by the successive explosions of trains of closely packed gas bubbles rather than a single large slug, or by flow oscillations related to the high speed motion of a compressible fluid and conduit irregularities. The sharp onset in echo power in the 344 m range gate for both P- and P+ shows that rising particles with motion components both toward and away from the antenna (pointing downward) contribute to the signal. The former are dominant as the bulk flow is vertically directed. The first break in slope is likely associated with ejecta leaving the gate through its upper boundary. P- then gently increases up to its peak amplitude nearly 3 s later, as more pyroclasts fill up the probed volume. About 6 s after the onset, P+ becomes dominant whereas P- starts to decrease, indicating the contribution from block fallout. Comparing with figure 11, it can be inferred that most of the

explosion momentum occurs during the first 6-7 s and corresponds to the main discharge of large ballistic blocks and dense lapilli- and ash-laden plume, with an initial maximum followed by a rapid decrease. The following phase, with lower velocities and echo power, results from the final emptying of the gas slug tail causing the relatively milder release of gas and finely fragmented ash at lower concentrations.

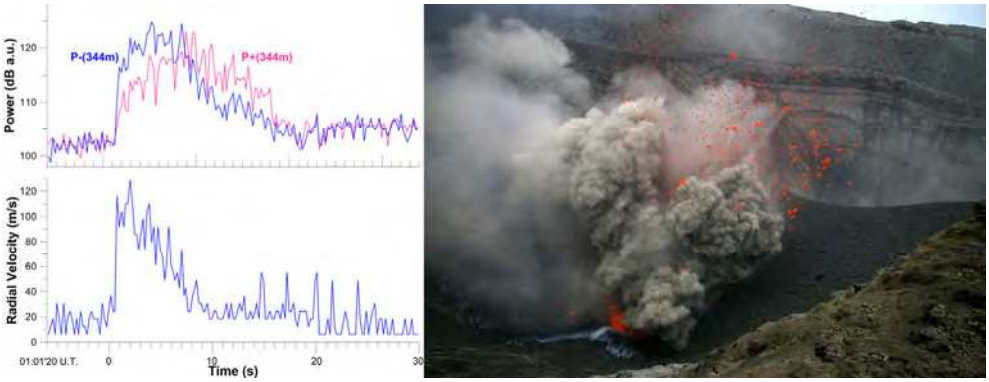

Fig. 10. (*left*): Time series of power (*top*) and maximum radial velocities (*bottom*) of a Strombolian outburst recorded by VOLDORAD aiming downward into Yasur's southern crater on 27/09/2008. Data are smoothed with 3 incoherent integrations (0.21 s).

Fig. 11. (*right*): Strombolian explosion at southern crater of Yasur volcano, Vanuatu. Incandescent pluridecimetric lava blocks resulting from the magma surface disruption by the pressurized gas slug are visible ahead of the ash plume (about a hundred meters high) generated by the magma fragmentation during gas pressure release. Photo courtesy: A. Finizola (2008).

5.2.4 Tephra mass loading

Gouhier & Donnadieu (2008) presented a method to estimate the particle loading parameters (mass, number, volume) of eruptive jets from the inversion of the echo power. The inversion algorithm uses the complete Mie (1908) formulation of electromagnetic scattering by spherical particles to generate synthetic backscattered power values. Assuming a log-normal shape for the particle size distribution, they estimated the total mass of tephra emitted during Strombolian explosions at Etna at around 58 and 206 tons for low and high concentration lava jets respectively. Derived parameters such as mass flux, particle kinetic and thermal energy, and particle concentration can also be estimated. As for particle concentrations, they must be regarded as minima in the case of small scale phenomena (relative to the range gate dimensions) like lava jets, because they are spatially highly heterogenous and might not completely fill the sounded volume. More reliable concentration values could be obtained when several range gates are filled completely, such as one expects from large ash plumes. For instantaneous events like Strombolian explosions, a total mass can be calculated from the echo power maximum amplitude assuming that all particles are present in the beam at the instant of the peak power. The instantaneous mass flux that can be derived in this way differs, however, from the initial mass flux as the power

peak does not occur at the signal onset (Fig. 10). The initial mass flux can be estimated from the mass corresponding to the first break in slope of the power curve (cf. 5.2.3.) divided by the time difference between the break in slope and the onset.

The particle size distribution being the main unknown, the tephra mass can be computed as a function of diameter for different reflectivity factors (Z). As seen from the curve shape in figure 12a, the uncertainty on mass is much less for lapilli and blocks than for ash at VOLDORAD's wavelength. This is also demonstrated in figure 12b: for a given tephra volume, Z is much lower for small particles and increases linearly with diameter (in log-log plot), up to particle diameters approaching a quarter of the wavelength (5.9 cm, end of the Rayleigh domain), and beyond this value fluctuates in a lower range. The curve in figure 12a corresponds to the value of Z calculated from the power peak amplitude of figure 10. It can be used to infer a minimum tephra mass of several tons for the high momentum first phase, reasonably assuming an average diameter for ballistic blocks of more than 4 cm. This leads to an initial mass flux of ≥10 tons/s for a period of low activity at Yasur, consistent with values of 26-74 tons/s found by Gouhier & Donnadieu (2008) for larger Strombolian outbursts at Etna.

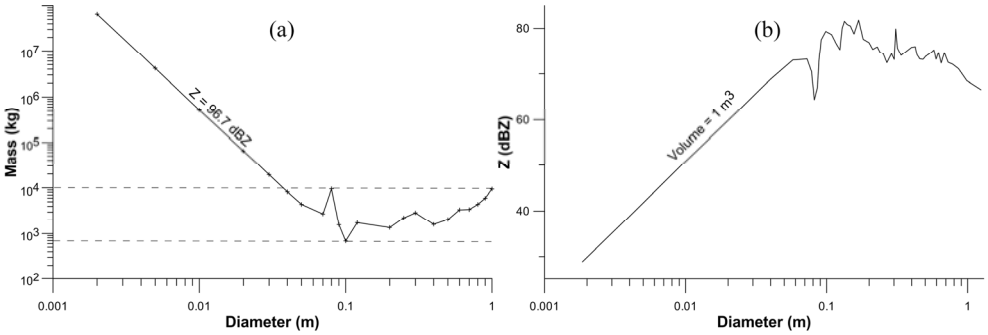

Fig. 12. (a) Tephra mass associated with a given reflectivity factor (Z), as a function of diameter. The curve shown corresponds to the value of Z calculated for the eruption of Yasur volcano in Fig.10. (b) Radar reflectivity factor associated with a tephra volume of 1 m^3, as function of diameter, calculated with sounding conditions at Arenal volcano.

For sustained tephra emissions, like ash plumes, the mass flux evolution could be tracked through an integration of the mass of rising particles over time. This is not straightforward, however, because (i) falling particles should be removed, (ii) the particle size distribution must be assumed to be constant with time, and (iii) the integration timestep is not the data acquisition rate that would otherwise cause redundance but is instead related to the average transit time of rising particles through the considered range gates, and (iv) all tephra are not ascending at the same velocity because of their wide range of sizes, and therefore they have different transit times, (v) the particle transit time will vary with time according to velocity variations (e.g. short-lived events). One method to retrieve the time variations of mass flux could be, at first order, to use the P+/P- ratio to find the proportion of rising particles and integrate the power-derived mass curve using as a timestep the range gate dimension along the flow direction divided by the bulk (power-weighted) flow velocity.

5.2.5 Gas flux estimates

Although maximum velocities measured by the radar result from particles, initial gas velocities can be estimated at first order using the corrections seen in section 5.2.2. and adequate model laws for the coupling of gas and particle velocities and gas velocity decrease with height. The volume and mass gas fluxes Q^g can also be estimated from the initial gas velocity (V_0^g) and vent section, the radius (r) of which can be observed in the field or inferred from modeling of acoustic signals:

$$Q_{vol}^g = \pi r^2 \times V_0^g \tag{11}$$

$$Q_{mass}^g = \rho^g \times Q_{vol}^g \tag{12}$$

where ρ^g is the gas density at the considered atmospheric pressure (elevation) and temperature; water vapor being the ultra-dominant species, its density can be used for ρ^g. Note that gas fluxes evolve similarly to the maximum radial velocities and therefore have a large peak at the explosion onset followed by a rapid decrease in a matter of seconds. Averaging over the duration of the emission for a large number of Strombolian explosions, Gouhier & Donnadieu (2011) found volume and mass gas fluxes of 3-11×10^3 m^3/s and 0.5-2 ton/s during the paroxysmal stage of a Strombolian eruptive episode of the SE crater at Etna. Radar-derived gas flux estimates at the source can then be compared with fluxes inferred from other ground-based techniques, like combined OP-FTIR gas spectroscopy and SO_2 flux measurements by DOAS, or ground-based thermal imagery.

6. Investigations of ash plumes with VOLDORAD

There is a continuum in the types of activity between Strombolian explosions seen previously and ash plumes. Ash plumes display a variety of behaviours depending on whether they are short-lived or sustained (steady state or not), whether they are jet plumes or buoyant plumes according to their momentum (mass loading, particle size distribution, fluxes), and also depending on environmental conditions including crosswind, elevation of the emission point, humidity and atmospheric temperature profiles, among the main ones. As an example, figure 13 shows three ash plumes with varying ash concentration and momentum, and also differently affected by the wind advection.

Fig. 13. Examples of various ash plumes at Arenal and Popocatépetl volcanoes. (a): low concentration buoyant plume bent over by wind advection at Arenal. (b): vertical jet plume, a few hundreds of meters in height, on same day (May 23, 2005). (c): dense ash plume of Popocatépetl buoyantly rising to about 2 km in height and drifting to the North on July 28 2007. Photos courtesy: Hotel Kioro Arenal and CENAPRED.

Ash is the major tephra component and is the main source of the ensuing hazards to humans, infrastructures and aviation, as shown by the 2010 eruption of Eyjafjallajökull in Iceland. This is because fine ash can remain in the atmosphere for hours to days, forming an ash cloud in the distal part. Although termed an ash plume, the proximal part does not comprise only ash, especially in the gas thrust and convective regions sounded by VOLDORAD. Below, examples are described which give insight into the ash plume dynamics close to the source.

6.1 Discriminating ballistics and ash

Tephra emissions are commonly explosive, having initial excess momentum compared with purely buoyant plumes. Therefore the explosive emission driven by the expansion of overpressured gas propels ash, lapilli and blocks in the air. Ash-sized particles closely follow the turbulent gas regime whereas inertial blocks mainly follow ballistic trajectories. So both are strongly decoupled, although a continuum of dynamic behaviors occurs in between for intermediary particle sizes. Because the spatiotemporal distribution of their velocity field and mass loading are contrasted, the dynamics of ballistics and ash can be discriminated when radar targeting the gas thrust region of the volcanic jet. Figure 14 illustrates the distinctive Doppler signatures for a jet plume at Arenal volcano similar to that shown in figure 13b and recorded with the beam aiming upward (27°) toward the summit. Although not obvious from the analysis of the time sequence of Doppler spectra the discrimination becomes particularly conspicuous on velocigrams. The velocigrams represent the power spectral density (dB color scale) as a function of radial velocities (y-axis) and time (x-axis) in 5 contiguous 120 m-wide range bins from 2367 to 2847 m. The 2607 m range bin, located above the vent, first records the jet plume onset. A 3-D representation of the velocigram at 2607 m is shown in the inset (cf. also book cover image). The ballistics are characterized by a short-lived signal (10-15 s) rapidly transiting through the gates. Range gates above the vent show positive radial velocities shifting to negative in a matter of seconds, as a result of the progressive bending of the ballistic trajectories through the radar beam.

Contrastingly, blocks only enter range gates located down-beam with negative radial velocities. So the time evolution of the spectral shape of this signal holds information about the ejection geometry (height, angles, orientation) and mass load spatial distribution, in addition to source parameters retrieved in section 5. Single streaks from individual blocks are sometimes visible on the velocigrams, and power-derived sizes are often decimetric. Considering lapilli to block sizes ranging between 0.04-1 m, Valade & Donnadieu (2011) found a mass of ballistics in the range 0.5–7 tons, i.e. a dense rock equivalent volume of 0.2-2.8 m^3, for a similar event at Arenal. The second signal characterizes the ash plume, with lower backscattered power (by 10-20 dB), longer duration (>1 mn), slower transit through the gates, and with only negative velocities because the wind pushes the ash toward the radar. Interestingly, these characteristic maximum radial velocities may be used to constrain the effect of the wind and the buoyant ascent velocity. Although clearly smaller than for ballistics, the particle size distribution in the ash plume is poorly constrained, and so is the ash mass. Also, the longer duration and wider spatial coverage of the ash cloud requires spatial and temporal integration to obtain the total mass, which is nevertheless presumably greater than the mass of ballistics.

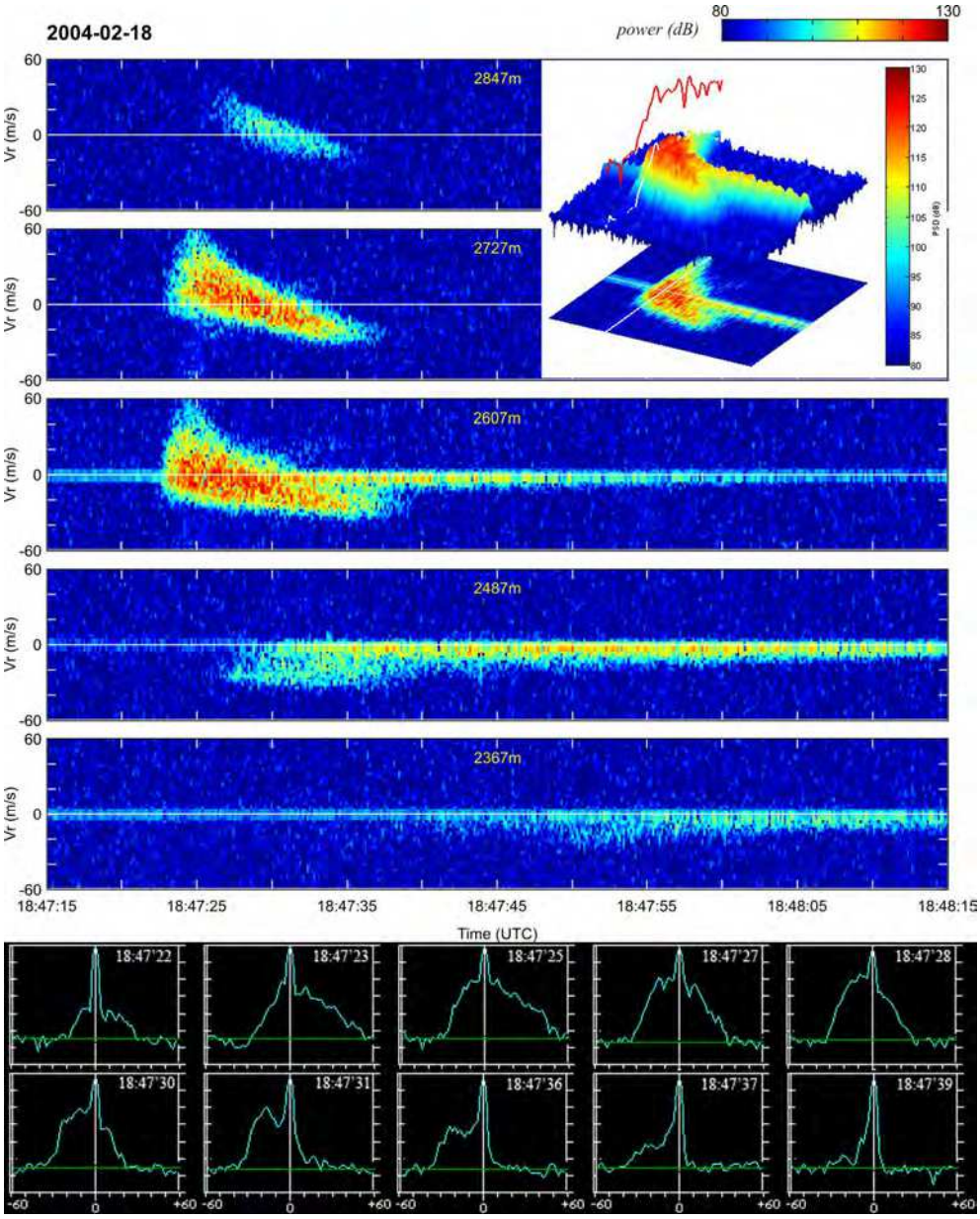

Fig. 14. Distinctive Doppler signatures of ballistics and ash dynamics for a jet plume at Arenal volcano (18/02/2004 at 18:47 U.T.). *Top*: velocigrams of 5 contiguous range bins. Inset: 3-D velocigrams of the 2607 m range bin above the vent. *Bottom*: Doppler spectra at 2607 m, showing power spectral density (dB arbitrary units) versus radial velocity (-60 to + 60 m/s); central peaks with constant power value are non filtered ground echoes.

6.2 Ash plume dynamics

The onset impulsivity of the same jet plume is nicely displayed on the time series of figure 15a, showing a sharp onset in maximum radial velocities, rapidly peaking over 80 m/s and then decreasing exponentially over about 10 seconds. The power maximum amplitude is also at the onset, indicating a mass flux maximum at the beginning, and P+ decreases rapidly after a few seconds and then more gently after about 10 s from the onset. The contribution of falling ballistics keeps P- high for a longer time. The 10 second phase of strong velocities and echo power corresponds to the initial mushroom-like ash plume head heavily charged with large blocks which dominate the signal. After this phase, radial velocities remain steady and low (10-20 m/s) and the power decreases more gently. The ballistics might therefore come from the disruption of the solidified lava plug by the gas overpressure accumulated underneath. This would clear the vent or fracture and open a way to a milder sustained gas release remobilizing variable quantities of ash and possibly fragmenting the lava to form juvenile ash.

Not all tephra emissions are impulsive at Arenal, and there are a wide variety of eruptive behaviors (Mora et al., 2009; Valade et al., 2012). Some emissions comprise mainly ash and are sustained typically for a minute or so (Fig. 15b). In contrast to the impulsive signal of jet plumes (Fig. 15a), the peak in echo power comes about 10 s after the onset. The second striking feature is the large oscillations correlated between P+ and P-, and having a remarkable periodicity of about 3 s. This indicates pulsations in the amount of material emitted, suggesting a staccato pressure release (Donnadieu et al., 2008). This observation supports the clarinet model of Lesage et al. (2006) for the volcanic tremor at Arenal, in which intermittent gas flow through fractures produces repetitive pressure pulses. The repeat period of the pulses is stabilized by a feedback mechanism associated with standing or traveling seismic waves in the magmatic conduit. Moreover, these rhythmic variations might well be a common feature of persistently active volcanoes with intermediate lava composition. In eruptions of Santiaguito volcano, Guatemala, Scharff et al. (2012) also observed multiple explosive degassing pulses occurring at intervals of 3-5 s, with common velocities of 20-25 m/s.

Figure 15c illustrates the signature of a larger ash plume of Popocatépetl, in Mexico, reaching a few kilometers above the volcano. Because its summit culminates at nearly 5450 m a.s.l., even small ash plumes generate hazards to the aviation, to the surrounding infrastructures and airports and the 30 million inhabitants leaving within 100 km of the volcano in important cities like México and Puebla. Its crater is 600 by 800 m wide with a growing lava dome inside. The relatively low velocities (<35 m/s) measured at 5085 m, along with the velocity peak not reached immediately after the onset, suggest low excess momentum and a mainly buoyant uprise, like most ash plumes in 2007 at Popocatépetl. Note that, in the case of ash plumes, radial velocities might reflect plume velocities more closely because convection and turbulence create eddies entraining particles that would tend to generate echoes with radial velocities toward and away from the radar, with comparable amounts of echo power in the absence of wind. From the time lag of P- relative to P+, however, it can be inferred that wind was blowing with some component toward the radar, i.e. to the north. In addition the power backscattered in 3 range gates simultaneously reveals that the horizontal dimension of the plume at the beam level was 2-3 times the radial resolution, i.e. >300 m. The comparable level of echo power at 5085 m and 5235 m, along

with the similar evolution of P+ at 5235 m and P- at 5085 m during the first seconds of the main emission indicate that the plume axis was near the boundary between these range gates, i.e. at a slant distance of 5160 m. This plus the fact that the main emission is shortly preceded by a weaker emission at 4935 m suggests that the ash plume originated from the northern part of the dome, closer to the radar.

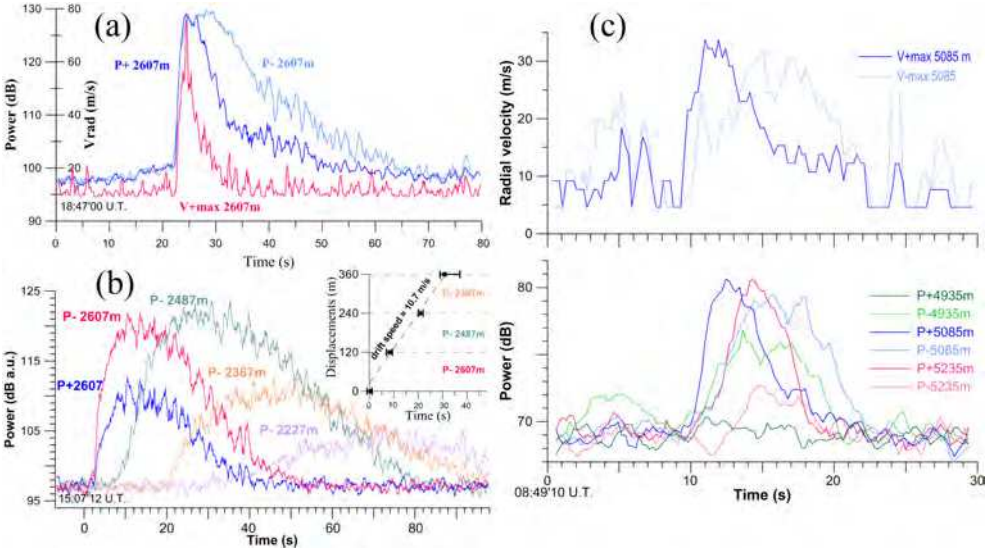

Fig. 15. Time series of echo power and velocities recorded by VOLDORAD (aiming upward) for (a) an impulsive jet plume (18/02/2004, 18:47) and (b) a sustained mild ash emission (11/02/2005, 15:07) at Arenal, and (c) a buoyantly rising ash plume at Popocatépetl (25/01/2007, 08:49).

6.3 Transport speed of ash plumes

The wind has a strong influence on ash plume dynamics, causing it to bend and, importantly for model-derived mass eruption rate estimates, be lower in height. When some wind component exists in the direction of the beam, radar echoes reflect the radial component of the drifting ash plume. As seen in figure 15b for a weak ash plume at Arenal, the near-source displacements of the plume can be tracked through echo onsets induced by ash entering successive probed volumes in the radar beam. When plotting the along-beam displacement versus time, a constant transport velocity is commonly reached within a few seconds of the initial ash emission (10.7 m/s along-beam in this case), as wind advection and buoyancy take over momentum. The departure of the first data point, i.e. the emission onset, from the general trend gives a relative indication of the slant distance of the vent to the radar. As shown by Donnadieu et al. (2011), the plume azimuth and uprise angles can further be constrained by comparing the amplitude decrease of the radar echoes as a function of distance from the source with results from a simple geometric plume model. This allows the three dimensional vector of the ash cloud transport speed to be reconstructed with an accuracy of a few percent. This method may have applications for determining pyroclasts fluxes, for

volcano monitoring, for the modeling of tephra dispersal, and for remote measurements of volcanic gas fluxes for which the plume transport speed is needed.

7. Other applications of transportable radars

Beyond their main use to measure near-source eruptive parameters, compact Doppler radars can be utilized for a number of other applications in volcano monitoring. The identification of erupting vents using range gating and the tracking of rockfalls are illustrated in this section; possible investigations on fallout are discussed in the concluding section.

7.1 Discrimination of active vents

The summit areas of active volcanoes have complex and evolving morphologies, often comprising multiple craters, themselves possibly nesting several vents, all potentially active simultaneously with various dynamics. The relatively good spatial resolution (tens of meters) of dedicated ground-based radars often allows the spatial discrimination of the surface activity and, in particular, the identification of the eruptive vents. This information is obviously very useful in volcano monitoring to locate the activity in real-time. Note that large wavelength signals, such as that used by VOLDORAD (L band) can penetrate through dense ash-laden plumes or lava fountains and give information on possible activity occurring in craters behind.

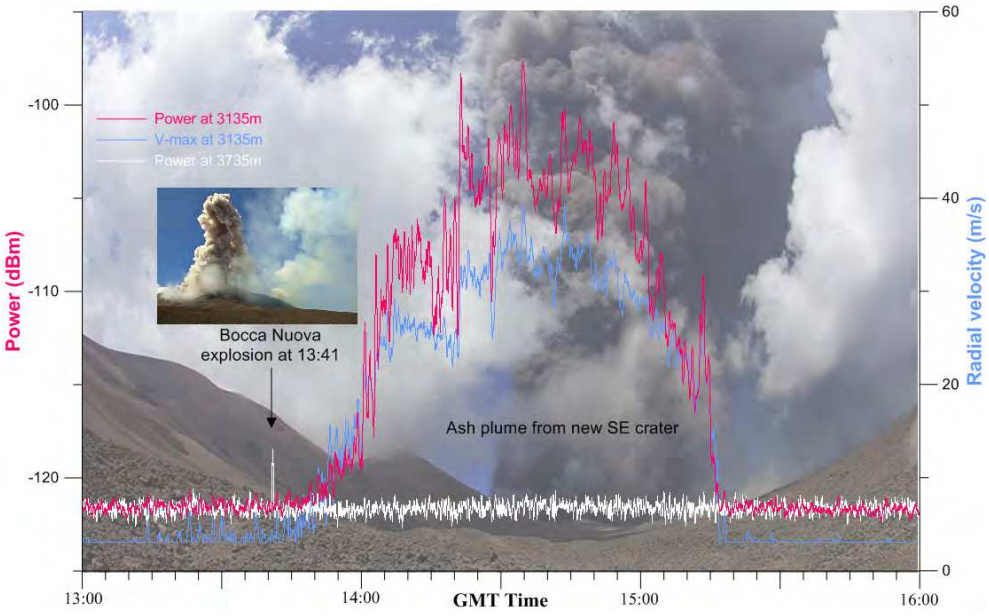

Fig. 16. Spatial discrimination of active craters of Etna using range gating (VOLDORAD 2B). Simultaneous tephra emissions of Bocca Nuova and new SE Crater at Etna on July 9 2011 are discriminated using echoes in range gates at 3735 m and 3135 m respectively (Radar data: OPGC-INGV; Photo courtesy: Tom Pfeiffer, www.volcanodiscovery.com).

At Etna, a ground-based Doppler radar operated jointly by the INGV in Catania and the OPGC in Clermont-Ferrand has been continuously monitoring the tephra emissions of the summit craters since 2009 (Donnadieu et al., 2009a, 2012) from a shelter at La Montagnola, about 3 km to the south. Echoes are recorded in 11 range bins, 150 m deep and 9° wide in azimuth and elevation, defining a 1650 m-long truncated conical volume covering the summit craters. These were very active in 2010-2012, showing different eruptive styles, including short-lived ash plumes (e.g. new SE Crater April 8 2010; Bocca Nuova, August 25 2010) and large ash columns several kilometers high sustained for several hours from lava fountains, such as the eruptive episodes of the new SE Crater in 2011 (Donnadieu, 2012; http://wwwobs.univ-bpclermont.fr/SO/televolc/voldorad/).

Figure 16 presents records from VOLDORAD 2B of simultaneous activity of Bocca Nuova and new SE Crater during cloudy weather. Radar monitoring is not hampered by clouds that sometimes make visual observations impossible. As shown by the echo power curves from the range gates at 3135 m and 3735 m, the short-lived explosion forming a weak plume at Bocca Nuova can be discriminated from the strong and dense column fed from the lava fountain originating in the new SE Crater and sustained for about 1.5 h. While the former cause a power increase of only a few dB, the latter result in much more powerful echoes (> 20 dB), with a progressive onset and more abrupt waning phase. Radial velocities in the convective ash and lapilli plume above the lava fountain commonly reach 30-40 m/s.

7.2 Tracking of rock falls

Not only the explosive activity can be monitored using transportable radars, but also lava flow or dome instabilities (Wadge et al., 2005; Hort el al., 2006). Viscous basaltic andesite lava flows continuously outpour from the summit of Arenal volcano and slowly flow on top of loose pyroclastic material down the steep and unstable upper slopes. Due to the joint actions of cooling and pushing by new lava, instabilities occur and generate repeated rock falls, sometimes evolving into small pyroclastic flows. While monitoring the ash emissions with VOLDORAD 2 from the west between January 26 and March 4 2009, signals from very frequent rock falls could be recorded in several range gates because their lowest part hit the volcano's upper slopes, where destabilizations occurred toward the SW.

The radar signature of rock falls is characterized by echoes with only radial velocity components toward the radar in contiguous bins at slant distances consistent with the location of the volcano's upper slopes (4013 and 3878 m on Fig.17). Radial velocities are typically low (<20 m/s). The amplitude of the backscattered power is less in closer bins, as expected if not all the destabilized material goes all the way down the slope. As seen from the power curves, signal onsets are delayed from the most remote range gates to the closest, as the destabilized material tumbles down. It is interesting that many small rock fall events detected by the radar are not always well recorded on seismograms, and thus both techniques appear complementary as noticed by Vöge et al. (2008).

An estimate of maximum block velocities during rock falls (V_{rf}) can be retrieved from the radial velocities (V_r) measured by the radar on the upper slopes when the geometry is known:

$$V_{rf} = V_r \times \frac{1}{\cos(\alpha)\cos(\theta_{rf} - \theta_{ant})} \tag{13}$$

where α is the azimuth difference between the rock fall direction and the beam axis, θ_{rf} the average angle of rock fall relative to the horizontal and θ_{ant} the elevation angle of the beam.

Approximate angle values determined from field observations ($\alpha \approx 45°$, $\theta_{rf} \approx 35°$, and $\theta_{ant} \approx 22°$ for the lowest part of the beam) lead to rock falls velocities equal to 1.45 times the measured radial velocities. With maximum radial velocities commonly in the range 7-14 m/s, the upper range of rock fall velocities is 10 to 20 m/s. Likewise, average rock fall speeds can be estimated from the time delays of power onsets in successive range gates and the gate radial resolution.

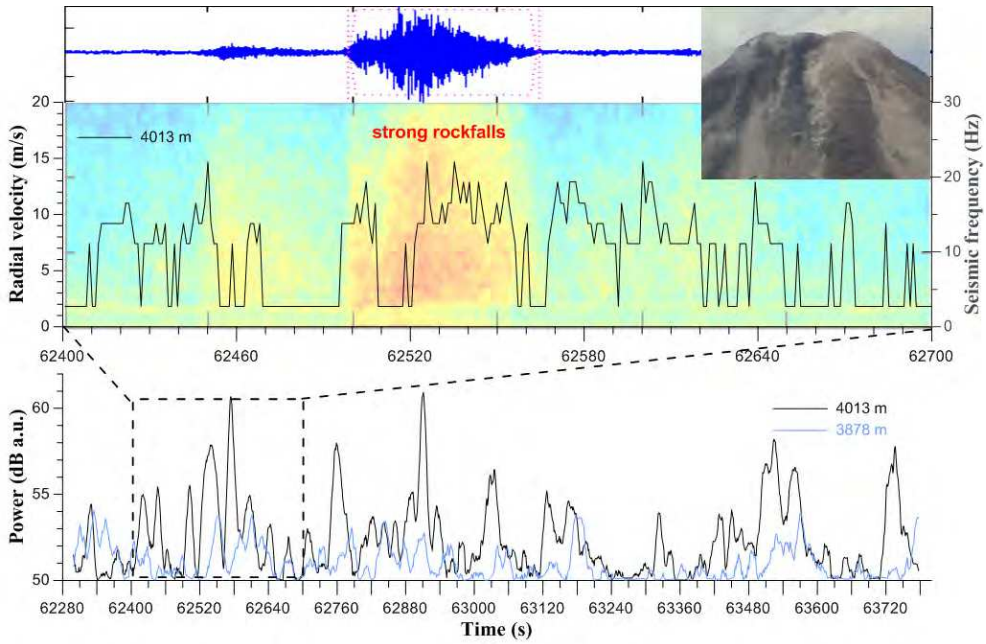

Fig. 17. Radar and seismic signals associated with rock falls at Arenal (02/02/2009). *Bottom*: 25 minute record of power from two range gates hitting the volcano upper slopes, where rock falls are detected by VOLDORAD; *middle*: maximum radial velocity (component towards radar) superimposed on a color spectrogram showing the seismic frequency content associated with rock fall events; *top*: seismic trace of a large rock fall and view of Arenal's summit from north showing lava flows and rock falls producing dust (seismic data courtesy of M. Mora; photo © F. Donnadieu, 14/05/2006).

In theory, the volume of rock falls could be determined from the power measured by the radar. In the case of Arenal, however, the size distribution of the fragments tumbling down the flanks is unknown and challenging to measure. Also, rock falls occurring in corridors can be masked by topographic obstacles or take place in other directions not visible to the radar so that it is likely that not all the falling material is detected and some events can even remain undetected by the radar. Nevertheless, as most rock falls are generated in

preferential directions during long periods of activity, transportable Doppler radars can be used to track this type of activity in order to assess the state of the activity, the stability of the lava flow or dome, and better understand the destabilization processes (Hort et al., 2006). They could be further used to correlate the rock fall activity, linked to the lava effusion rate, to the emissions of tephra. As both types of event could be recorded by the radar, such a comparative quantified analysis over a representative time sequence spanning several weeks could provide information on the eruptive behavior of the volcano and the dynamics of its upper plumbing system.

8. Conclusion and future prospects

Illustrations provided in this chapter show the many capabilities of Doppler radars to investigate and monitor volcanic phenomena in real-time and in all weather conditions. The L-band portable volcano Doppler radar of the OPGC is particularly useful for monitoring explosive activities of variable intensity from a chosen location. Owing to its 23.5 cm wavelength, VOLDORAD is able to sound the interior of dense particle-laden volcanic jets. By directly probing the jets near the vent, quantified eruption source parameters can be retrieved in different volumes with a high spatiotemporal resolution.

A major challenge in the mitigation of ash plume-related risks is to determine the relative mass flux of volcanic material propelled into the atmosphere, in particular the mass transport rate in the cloud at the neutral buoyancy level. The mass transport rate represents only a fraction of the total flux of magma erupted at the vent (magma mass eruption rate), which also includes the effusive activity (lava flows, lava dome) as well as all the lava falling back into the crater and its immediate surroundings contributing to the growth of pyroclastic cones (e.g. ballistics). The proportion of material propelled into the atmosphere strongly controls the hazards to humans and infrastructures, the economic costs and environmental consequences, but also represents an essential input to volcanic ash transport and dispersion models. Its estimation in near real-time could allow models to be constantly refined by comparing their predictions with measurables from ground-based and satellite remote sensing methods and ground deposit data. Model inputs from deposit observations (e.g. thickness) to quantify eruption characteristics cannot be done in real-time as this requires the collection of many fallout samples at remote locations. Although models allow the tephra mass flux to be estimated from the ash column height, the latter needs to be accurately measured and defined, in particular with regard to the strong effect of crosswinds. This can be achieved most reliably through a combination of methods, but radars appear particularly relevant in this case. Weather radars can provide the plume height, within the uncertainties discussed in section 2, along with characteristics of the ash cloud including transport speed estimates. Compact Doppler radars sounding the plume base at a high acquisition rate should help discriminate the mass eruption rate from the mass transport rate and link models of plume ascent to models of tephra dispersal by providing crucial source kinetic and mass loading parameters. The radar echo power is also related to the amount of material ejected and can be inverted to retrieve the mass. Among the most stringent assumptions for this is the particle size distribution in the sounded volumes. It can be inferred from direct measurements of fallout (rain radar, disdrometer etc) or deposit sampling, in situ sampling by aircraft, or comparison with data from similar

eruptions. We could more ambitiously imagine vertical soundings by transportable Doppler radars from underneath wind-advected ash clouds to provide the vertical distribution of both the particle concentration and fallout velocities, owing to their directive antenna and range gating capability. Tracking the time evolution of these parameters would give access to the internal dynamics of ash clouds and sedimentation processes. Terminal fall velocities could in turn be related to the particle size distribution that could be compared with field deposits and results from tephra dispersal models. Fallout measurements from ground collectors and several continuously operating laser or microwave disdrometers would improve understanding of the relationship between particle size and fall velocity, and the spatial heterogeneities often observed in ground deposits.

Unfortunately, a comprehensive real-time technique that can provide the erupted mass associated with the whole particle-size spectrum does not yet exist. This could only be derived from a combination of complementary techniques. This argues for a synergetic strategy for the assimilation of multiple datasets quantitatively describing the different parts of a plume from the gas-thrust region through the convective region to the buoyant distal cloud. As described in this chapter, the proximal region can be well quantified by radars, and developments are expected with multiple/complementary frequencies and dual polarimetry. The cross-correlation of data from radars and complementary passive remote-sensing methods, particularly ground-based imagery (IR, VIS, UV), is also a potentially powerful tool to retrieve crucial parameters like particle size distribution, gas and tephra mass fluxes. Ground-based radars are not useful for long-term volcanic cloud tracking because the large ash particles, that provide strong radar signals fall out soon after an eruption. C-band radars, for instance, do not detect ash particles with diameter <1-100 μm in drifting volcanic clouds that can persist in the atmosphere for several days or more (Rose et al., 1995). Thus, for the long-range tracking of ash clouds, satellite-based imagers (IR, VIS, UV, microwave) bring an obvious synergetic contribution, along with MISR and lidars, more sensitive to micron- to submicron-sized particles and aerosols, ceilometers, sun photometers, and DOAS mainly for SO_2. An important objective of future works should aim at comparing and calibrating data from different instruments and/or acquired at different wavelengths, always cross-validated with field data (e.g. Bonadonna et al., 2011, 2012; Donnadieu et al., 2009b; Gouhier et al., 2011). Further coupling with other geophysical methods, in particular seismic and acoustic, seems promising to investigate the eruptive behavior of a volcano from down the conduit up through the magma-air interface where explosions occur, up to the surface where the dynamics of the tephra emissions can be recorded. Finally, back to figure 1, the synergetic integration of source-targeting Doppler radars, medium-range weather radars (few tens-hundreds km), and satellite- and ground-based imagery, combined with traditional monitoring networks and field methods, is a promising approach to improve the assessment of ash plume-related hazards, the forecast from tephra dispersal models and the mitigation of associated risks. In order to retrieve accurate eruption parameters, future research should focus on joint measurements of ash plume characteristics at different levels by means of complementary techniques. To this purpose, a good strategy would be to (i) carry out well-targeted multi-method experiments on volcanoes showing either recurrent activity or sudden resumption of activity, and (ii) operate long-term observations at selected laboratory volcanoes having a well-instrumented monitoring network.

9. Acknowledgments

I am much indebted to the OPGC staff for developments of the radar system, in particular G. Dubosclard, R. Cordesses, C. Hervier, J. Fournet-Fayard, P. Fréville, C. Bernard, C. Reymond, and for implementation of databases (S. Rivet, P. Cacault). I am also grateful to C. Hervier, T. H. Druitt, M. Gouhier, S. Valade for assistance in data acquisition in the field, and to E. Bonny, A. Clenet, J. Doloire, M. Gouhier, A. Maillet, L. Perrier, L. Pouchol, N. Rodriguez, S. Saumet, D. Tailpied, P. Tinard and S. Valade for help in data processing of the different campaigns. Y. Pointin kindly provided data on meteorological signals. All these colleagues are warmly acknowledged. External partners facilitated radar soundings: Universidad de Costa Rica (M. Mora, G. Alvarado, L.-F. Brenes, F. Arias and C. Ramirez), DGMWR in Port Vila Vanuatu (E. Garaebiti, C. Douglas), UNAM-CENAPRED in Mexico. Radar measurements from VOLDORAD 2B on Etna were obtained in the frame of a collaboration between OPGC and INGV Catania (M. Coltelli, S. Scollo, M. Prestifilippo). Field campaigns were supported by the French CNRS INSU programs 2003-ACI Risques Naturels, ANR-06-CATT-02 Arc-Vanuatu, 2010-TERMEX-MISTRALS, 2011-2012 CT3, and by the European project VOLUME FP6-018471.

This is Laboratory of Excellence *CLERVOLC* contribution n° 12.

10. References

Adams, R.J., Perger, W.F., Rose, W.I., & Kostinski, A. (1996). Measurements of the complex dielectric constant of volcanic ash from 4 to 19 GHz. *J. Geophys. Res*., 101, B4, pp. (8175-8185).

Arason, P., Petersen, G. N., Bjornsson, H. (2011). Observations of the altitude of the volcanic plume during the eruption of Eyjafjallajökull, April–May 2010. Earth Syst. Sci. Data, 3, pp. (9–17).

Arason, P., Bjornsson, H., Petersen, G. N., Roberts, M. J., & Collins M. (2012). Resonating eruptive flow rate during the Grímsvötn 2011 volcanic eruption. *30th Nordic geological winter meeting*, 9-12 January 2012, Reykjavík, Iceland.

Bonadonna, C., Folch, A., Loughlin, S., Puempel, H. (2012). Future developments in modelling and monitoring of volcanic ash clouds: outcomes from the first IAVCEI-WMO workshop on Ash Dispersal Forecast and Civil Aviation. *Bull. Volcanol*., 74, 1, pp. (1-10).

Bonadonna, C., Genco, R., Gouhier, M., Pistolesi, M., Cioni, R., Alfano, F., Hoskuldsson, A., & Ripepe M. (2011). Tephra sedimentation during the 2010 Eyjafjallajökull eruption (Iceland) from deposit, radar, and satellite observations. *J. Geophys. Res*., 116, B12202.

Casagli, N., Tibaldi, A., Merri, A., Del Ventisette, C., Apuani, T., Guerri, L., Fortuny-Guasch, J., & Tarchi D. (2009). Deformation of Stromboli Volcano (Italy) during the 2007 eruption revealed by radar interferometry, numerical modelling and structural geological field data. *J. Volcanol. Geotherm. Res*., 182, pp. (182–200).

Campbell, M.J., & Ulrichs, J. (1969). Electrical properties of rocks and their significance of Lunar Radar Observations. *J. Geophys. Res*., 74, 25, pp. (5867-5881).

Delene, D.J., Rose, W.I., & Grody, N.C. (1996). Remote sensing of volcanic clouds using special sensor microwave imager data. *J. Geophys. Res.,* 101, B5, pp. (11579-11588).

Donnadieu, F., Dubosclard, G., Allard, P., Cordesses, R., Hervier, C., Kornprobst, J., & Lénat, J.-F. (2003). Sondages des jets volcaniques par radar Doppler : applications à l'Etna. *Rapport quadriennal C.N.F.G.G. 1999-2002*, pp. (119-124).

Donnadieu, F., Dubosclard, G., Cordesses, R., Druitt, T.H., Hervier, C., Kornprobst, J., Lénat, J.-F., Allard, P., & Coltelli, M. (2005). Remotely monitoring volcanic activity with ground-based Doppler radar. *E.O.S. Trans*., 86, 21, pp. (201-204).

Donnadieu F., Gouhier M., Fournet-Fayard J., Hervier C., 2008. Applications of pulsed ground-based Doppler radar to the study and monitoring of volcanoes, Ground-based radar observations for volcanoes workshop, Univ. Reading UK, pp. (6-8).

Donnadieu, F., Hervier, C., Fréville, P., Fournet-Fayard, J., Fournol, J.-F., Menny, P., Reymond, C., & Bernard, C. (2009a). The VOLDORAD 2B radar: Operational handbook, Note OPGC 07.09, Univ. Blaise Pascal Clermont-Ferrand.

Donnadieu F., Roche O., Clarke A., Gurioli L., (2009b). Advances in studies of volcanic plumes and pyroclastic density currents. Report of the IAVCEI Commission on Explosive Volcanism, workshop in Clermont-Ferrand (France), 26-29 October 2009, 18pp.

Donnadieu, F., Valade, S., & Moune, S. (2011). Three dimensional transport speed of wind-drifted ash plumes using ground-based radar. *Geophys. Res. Lett*., 38, L18310, doi:10.1029/2011GL049001.

Donnadieu, F. (2012). VOLDORAD, In: *Observatoire de Physique du Globe de Cleront-Ferrand web site*, 2012, < http://wwwobs.univ-bpclermont.fr/SO/televolc/voldorad/>.

Donnadieu, F., Coltelli, M., Scollo, S., Fréville, Hervier, C., P., Prestifilippo, M., Rivet, S., Cacault, P., Fournet-Fayard, J., Bernard, C., & Reymond, C. (2012). Doppler radar monitoring of the explosive activity at Etna's summit craters with VOLDORAD 2B: toward an integrated approach. MEMOVOLC meeting, Jan. 17-18, Clermont-Ferrand, France.

Doviak, R. J. and D. S. Zrni´c, 1993: Doppler Radar and Weather Observations. Academic Press. Cambridge University Press, 562 pp.

Dubosclard, G., Cordesses, R., Allard, P., Hervier, C., Coltelli, M., & Kornprobst, J. (1999). First testing of a volcano Doppler radar (Voldorad) at Mount Etna, Italy. *Geophys. Res. Lett.,* 26, pp.(3389-3392).

Dubosclard G., Donnadieu, F., Allard, P., Cordesses, R., Hervier, C., Coltelli, M., Privitera, E., & Kornprobst, J. (2004). Doppler radar sounding of volcanic eruption dynamics at Mount Etna. *Bull. Volcanol.*, 66, 5, pp. (443-456), DOI : 10.1007/s00445-003-0324-8.

Froger, J.-L., Remy, D., Bonvalot, S. and Legrand, D. (2007). Two scales of inflation at Lastarria-Cordon del Azufre volcanic complex, central Andes, revealed from ASAR-ENVISAT interferometric data. *Earth Planet. Sc. Lett*. 255, pp. (148-163).

Gerst, A., Hort, M. Kyle, P. R., & Vöge, M. (2008). 4D velocity of strombolian eruptions and man-made explosions derived from multiple Doppler radar instruments. *J. Volcanol. Geotherm. Res.*, 177 (3), pp. (648–660),

doi:10.1016/j.jvolgeores.2008.05.022.

Gouhier, M., Harris, A., Calvari, S., Labazuy, P., Guéhenneux, Y., Donnadieu, F., & Valade, S. (2011). Lava discharge during Etna's January 2011 fire fountain tracked using MSG-SEVIRI. *Bull. Volcanol., in press*.

Gouhier, M., & Donnadieu, F. (2008). Mass estimations of ejecta from Strombolian explosions by inversion of Doppler-radar measurements. *J. Geophys. Res*., 113, B10202, doi:10.1029/2007JB005383.

Gouhier, M., & Donnadieu, F. (2010). The geometry of Strombolian explosions: insight from Doppler radar measurements. *Geophys. J. Int.*, 183, pp. (1376–1391), doi: 10.1111/j.1365-246X.2010.04829.x

Gouhier, M., & Donnadieu, F. (2011). Systematic retrieval of ejecta velocities and gas fluxes at Etna volcano using L-Band Doppler radar. *Bull. Volcanol.,* 73, pp. (1139–1145).

Hannesen, R., & Weipert, A. (2011). An algorithm to detect and quantify volcanic eruptions using polarimetric X-band radar data. Int. Workshop on X-band Weather Radar, 14-16 Nov. 2011, Delft, Netherlands.

Harris, D. M., Rose, W.I.Jr., Roe, R., & Thompson, M.R. (1981). Radar observations of ash eruptions. In: *The 1980 Eruptions of Mount St. Helens, Washington*, edited by P. W. Lipman and D. R. Mullineaux, U.S. Geol. Surv. Prof. Pap. 1250, pp. (323-333).

Harris, D. M., & Rose, W.I.Jr. (1983). Estimating particle sizes, concentrations, and total mass of ash in volcanic clouds using weather radar. *J. Geophys. Res*., 88, C15, pp. (10969–10983), doi:10.1029/JC088iC15p10969.

Hoblitt, R. P., & Schneider, D. J. (2009). Radar observations of the 2009 eruption of Redoubt Volcano, Alaska: Initial deployment of a transportable Doppler radar system for volcano-monitoring. American Geophysical Union, Fall Meeting 2009, abstract #V43A-2209.

Hort, M., & Seyfried, R. (1998). Volcanic eruption velocities measured with a micro radar. Geophys. Res. Lett. 25, 1, pp.(113–116).

Hort, M., Seyfried, R., & Vöge M. (2003). Radar Doppler velocimetry of volcanic eruptions: theoretical considerations and quantitative documentation of changes in eruptive behaviour at Stromboli Volcano, Italy. *Geophys. J. Int., 154,* pp. (515–532), doi:10.1046/j.1365-246X.2003.01982.x.

Hort, M., Vöge, M., Seyfried, R., & Ratdomopurbo, A. (2006). In situ observation of dome instabillities at Merapi Volcano, Indonesia: A new tool for hazard mitigation. *J. Volcanol. Geotherm. Res*., 153, pp. (301–312), doi:10.1016/j.jvolgeores.2005.12.007.

Lacasse, C., Karlsdóttir, S., Larsen, G., Soosalu, H., Rose, W. I., & Ernst, G.G.J. (2004). Weather radar observations of the Hekla 2000 eruption cloud, Iceland. *Bull. Volcanol*., 66, pp. (457–473), doi:10.1007/s00445-003-0329-3.

Lesage, P., Mora, M.M., Alvarado, G.E., Pacheco, J., & Métaxian J.-P. (2006). Complex behavior and source model of the tremor at Arenal volcano, Costa Rica. *J. Volcanol. Geotherm. Res*., 157, pp. (49–59).

Macfarlane, D. G., Wadge, G., Robertson, D. A., James, M. R., & Pinkerton, H. (2006). Use of a portable topographic mapping millimeter wave radar at an active lava flow. *Geophys. Res. Lett*., 33, L03301, doi:10.1029/2005GL025005.

Maki M., & Doviak, R. J. (2001). Volcanic ash size distribution determined by weather radar. *IEEE Int. Geosc. Rem. Sens. Symp., IGARSS '01.*, 2001, vol.4, pp. (1810 – 1811), doi: 10.1109/IGARSS.2001.977079.

Maki M., Iwanami, K., Misumi, R., Doviak, R. J., Wakayama, T., Hata, K., & Watanabe, S. (2001). Observation of volcanic ashes with a 3-cm polarimetric radar. *Proc. 30th Radar Meteorol. Conf.*, 18-24 July, Munich, Germany, P5.13, p. (226-228).

Malassingne, C., Lemaitre, F., Briole, P., & Pascal, O. (2001). Potential of ground based radar for the monitoring of deformation of volcanoes. *Geophys. Res. Lett*. 28, 851–854.

Marzano, F.S., & Ferrauto, G. (2003). Relation between weather radar equation and first-order backscattering theory. *Atmos. Chem. Phys*., 3, pp. (813–821).

Marzano, F. S., Barbieri, S., Vulpiani G., & Rose W.I. (2006a). Volcanic ash cloud retrieval by ground-based microwave weather radar. *IEEE Trans. Geosc. Remote Sens.*, 44 (11), pp. (3235–3246), doi:10.1109/TGRS.2006.879116.

Marzano, F.S., Vulpiani, G., & Rose W.I. (2006b). Microphysical characterization of microwave radar reflectivity due to volcanic ash clouds. *IEEE Trans. Geosc. Remote Sens.*, 44, pp. (313–327), doi:10.1109/TGRS.2005.861010.

Marzano, F.S., Barbieri, S., Picciotti, E., & Karlsdóttir, S. (2010a). Monitoring sub-glacial volcanic eruption using C band radar imagery. *IEEE Trans. Geosc. Remote Sens.*, 48, 1, pp. (403-414).

Marzano, F. S., Marchiotto, S., Barbieri, S., Textor, C., & Schneider, D. (2010b). Model-based Weather Radar Remote Sensing of Explosive Volcanic Ash Eruption, *IEEE Trans. Geosc. Remote Sens.*, 48, pp. (3591-3607).

Marzano, F. S., Lamantea, M., Montopoli, M., Di Fabio, S., & Picciotti, E. (2011). The Eyjafjöll explosive volcanic eruption from a microwave weather radar perspective. *Atmos. Chem. Phys. Discuss.*, 11, pp. (12367–12409), doi:10.5194/acpd-11-12367-2011.

Marzano, F. S., Picciotti, E., Vulpiani, G., & Montopoli, M. (2012). Synthetic signatures of volcanic ash cloud particles from X-band dual-polarization radar. *IEEE Trans. Geosc. Remote Sens.*, 50, 1, pp. (193-211).

Mastin, L. G., Guffanti, M., Servranckx, R., Webley, P., et al. (2009). A multidisciplinary effort to assign realistic source parameters to models of volcanic ash cloud transport and dispersion during eruptions. *J. Volcanol. Geotherm. Res*., 186, pp. (10–21).

Mie, G. (1908). Beiträge zur Optik trüber Medien, speziell kolloidaler Metallösungen. *Ann. Phys*., 330, 3, pp. (377–445).

Mora, M.M., Lesage, P., Donnadieu, F., Valade, S., Schmidt, A., Soto, G., Taylor, W., & Alvarado, G. (2009). Joint Seismic, Acoustic and Doppler Radar observations at Arenal Volcano, Costa Rica: preliminary results. In: *The VOLUME project*, Bean, C. J., Braiden, A. K., Lokmer, I., Martini, F., & O'Brien, G. S. , pp. (330-340), VOLUME Project Consortium, ISBN 978-1-905254-39-2, Dublin.

Musolf,M. (1994). Airborne radar detection of volcanic ash. *In*: First International Symposium on Volcanic Ash and Aviation Safety, Casadevall, T.J. (Ed.), *U.S. Geol. Surv. Bull., 2047*, pp. (387–390), Seattle, Washington, U.S.A.

Oguchi, T., Udagawa, M., Nanba, N., Maki, M., & Ishimine, Y. (2009). Measurements of dielectric constant of volcanic ash erupted from five volcanoes in Japan. *IEEE Trans. Geosc. Remote Sens.*, 47, 4, pp. (1089 - 1096).

Okamato, H. (2002). Information content of the 95-GHz cloud radar signals: Theoretical assessment of effects of non sphericity and error evaluation of the discrete dipole approximation. *J. Geophys. Res.*, 107, D22, 4628.

Oswalt, J. S., Nichols, W., & O'Hara, J. F. (1996). Meteorological observations of the 1991 Mount Pinatubo eruption, In: *Fire and Mud: Eruptions and Lahars of Mount Pinatubo, Philippines*, Newhall C. G., & Punongbayan R. S., pp. (625–636), Univ. of Wash. Press, Seattle.

Prata, F., Bluth, G., Rose, W.I., Schneider, D., & Tupper, A. (2001). Comments on 'Failures in detecting volcanic ash from a satellite-based technique'. *Remote Sens. Environ.*, 78, 3, pp. (341–346).

Rogers, A.B., Macfarlane, D.G., Robertson, D.A. (2011). Complex permittivity of volcanic rock and ash at millimeter wave frequencies. *IEEE Remote Sens. Lett.*, 8, 2, pp. (298-302).

Rose, W.I., Kostinski, A.B. (1994). Radar remote sensing of volcanic clouds. *In*: First International Symposium on Volcanic Ash and Aviation Safety, Casadevall, T.J. (Ed.), *U.S. Geol. Surv. Bull.*, 2047, pp. (391–395), Seattle, Washington, U.S.A.

Rose, W. I., Kostinski, A. B., & Kelley, L. (1995). Real-time C band radar observations of 1992 eruption clouds from Crater Peak vent, Mount Spurr Volcano, Alaska. *In*: The 1992 eruptions of Crater Peak vent, Mount Spurr Volcano, Alsaka, Keith, T. (Ed.), pp. (19-26), *U.S. Geol. Surv. Bull.*, 2139.

Rose, W. I., Bluth, G. J. S., & Ernst, G. G. J. (2000). Integrating retrievals of volcanic cloud characteristics from satellite remote sensors—A summary. *Phil. Trans. R. Soc. A*, vol. 358, 1770, 1585–1606.

Russell, J. K., & Stasiuk, M. V. (1997). Characterization of volcanic deposits with ground-penetrating radar. *Bull. Volcanol.*, 58, pp. (515–527).

Sauvageot, H. (1992). *Radar meteorology*, Artech House, ISBN 0890063184, Boston.

Scharff, L., M. Hort, A. J. Harris, M. Ripepe, J. Lees, and R. Seyfried (2008), Eruption dynamics of the SW crater of Stromboli volcano, Italy. *J. Volcanol. Geotherm. Res.*, *176*, pp. (565–570).

Scharff, L., Ziemen, F., Hort, M., Gerst, A., & Johnson J.B. (2012). A Detailed View Into the Eruption Clouds of Santiaguito Volcano, Guatemala, Using Doppler radar. *J. Geophys. Res.*, in revision.

Schneider, D.J. (2009). Explosive volcanic eruptions: what can radar do for you? *2d Nat. Symp. on Multifunction Phased Array Radar*, November 18-20, 2009, Norman, OK, USA.

Schneider, D.J. (2012). The Use of a Dedicated Volcano Monitoring Doppler Weather Radar for Rapid Eruption Detection and Cloud Height Determination. *92nd American Meteorological Society Annual Meeting*, Jan. 22-26 2012, New Orleans, LA, USA.

Scollo, S., Coltelli, M., Prodi, F., Folegani, M., & Natali, S. (2005). Terminal settling velocity measurements of volcanic ash during the 2002–2003 Etna eruption by an X-band

microwave rain gauge disdrometer. *Geophys. Res. Lett.,* 32, L10302, doi:10.1029/2004GL022100.

Scollo, S., Prestifilippo, M., Spata, G., D'Agostino, M., & Coltelli, M. (2009). *Nat. Hazards Earth Syst. Sci*., 9, pp. (1573–1585).

Scollo, S., Folch, A., Coltelli, M., & Realmuto, V. J. (2010). Three-dimensional volcanic aerosol dispersal: A comparison between Multiangle Imaging Spectroradiometer (MISR) data and numerical simulations. *J. Geophys. Res*., 115, D24210.

Seyfried, R., & Hort, M. (1999). Continuous monitoring of volcanic eruption dynamics: A review of various techniques and new results from a frequency-modulated radar Doppler system. *Bull. Volcanol*., 60, pp. (627–639).

Stone, M. (1994). Application of contemporary ground-based and airborne radar for the observation of volcanic ash. *In*: First International Symposium on Volcanic Ash and Aviation Safety, Casadevall, T.J. (Ed.), U.S. Geol. Surv. Bull., 2047, pp. (391–395), Seattle, Washington, U.S.A.

Valade, S. & Donnadieu, F. (2011). Ballistics and ash plumes discriminated by Doppler radar. *Geophys. Res. Lett.,* 38, L22301, doi:10.1029/2011GL049415.

Valade, S., Donnadieu, F., Lesage, P., Mora, M.M., Harris, A. & Alvarado, G.E. (2012). Explosion mechanisms at Arenal volcano, Costa Rica: an interpretation from integration of seismic and Doppler radar data. *J. Geophys. Res*., 117, B1, doi:10.1029/2011JB008623.

Vöge, M., & Hort, M. (2008). Automatic classification of dome instabilities based on Doppler radar measurements at Merapi volcano, Indonesia: Part I. *Geophys. J. Int.*, *172*, pp. (1188–1206), doi:10.1111/j.1365-246X.2007.03605.x.

Vöge, M., Hort, M., Seyfried, R., Ratdomopurbo, A. (2008). Automatic classification of dome instabilities based on Doppler radar measurements at Merapi volcano, Indonesia: Part II. *Geophys. J. Int.*, *172*, pp. (1207–1218), doi:10.1111/j.1365-246X.2007.03665.x.

Vöge, M., & Hort, M. (2009). Installation of a Doppler Radar monitoring system at Merapi Volcano, Indonesia. *IEEE Trans. Geosc. Remote Sens*., 47, 1, pp. (251–271), doi:10.1109/TGRS.2008.2002693.

Vulpiani, G., Montopoli, M., Piccioti, E., & Marzano F.S. (2011). On the use of a polarimetric X-band weather radar for ash clouds monitoring. *Proc. 35th Radar Meteorol. Conf*., 26-30 September, Pittsburgh, PA, USA, P.101.

Wadge, G., Macfarlane, D.G., Robertson, D.A., Hale, A.J., Pinkerton, H., Burrell, R.V., Norton, G. E., & James, M.R. (2005). AVTIS: A novel millimetre-wave ground based instrument for volcano remote sensing. *J. Volcanol. Geotherm. Res*., 146, 307–318.

Wadge, G., Macfarlane, D.G., Odbert, H.M., James, M.R., Hole, J.K., Ryan, G., Bass, V., De Angelis, S., Pinkerton, H., Robertson, D.A., & Loughlin, S. C. (2008). Lava dome growth and mass wasting measured by a time series of ground-based radar and seismicity observations. J. Geophys. Res., 113, B08210, doi:10.1029/2007JB005466.

Wen, S., & Rose, W.I. (1994). Retrieval of sizes and total masses of particles in volcanic clouds using AVHRR bands 4 and 5. *J. Geophys. Res*., 99, pp. (5421-5431).

Weill, A., Brandeis, G., & Vergniolle, S. (1992). Acoustic sounder measurements of vertical velocity of volcanic jets at Stromboli volcano. *Geophys. Res. Lett*., 19, 23, pp. (2357-2360).

Wood, J., Scott, C., & Schneider, D. (2007). WSR-88D radar observations of volcanic ash. WorldMeteorological Organization, *Proc. 4th Int. Workshop Ash*, Mar. 26–30, 2007, Rotorua, New Zealand.

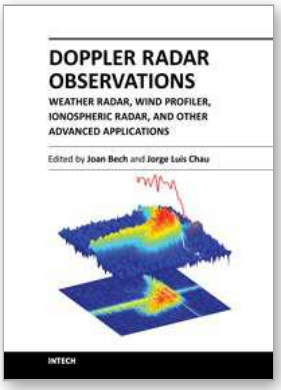

Doppler Radar Observations - Weather Radar, Wind Profiler, Ionospheric Radar, and Other Advanced Applications

Edited by Dr. Joan Bech

ISBN 978-953-51-0496-4
Hard cover, 470 pages
Publisher InTech
Published online 05, April, 2012
Published in print edition April, 2012

Doppler radar systems have been instrumental to improve our understanding and monitoring capabilities of phenomena taking place in the low, middle, and upper atmosphere. Weather radars, wind profilers, and incoherent and coherent scatter radars implementing Doppler techniques are now used routinely both in research and operational applications by scientists and practitioners. This book brings together a collection of eighteen essays by international leading authors devoted to different applications of ground based Doppler radars. Topics covered include, among others, severe weather surveillance, precipitation estimation and nowcasting, wind and turbulence retrievals, ionospheric radar and volcanological applications of Doppler radar. The book is ideally suited for graduate students looking for an introduction to the field or professionals intending to refresh or update their knowledge on Doppler radar applications.

InTech Europe
University Campus STeP Ri
Slavka Krautzeka 83/A
51000 Rijeka, Croatia
Phone: +385 (51) 770 447
Fax: +385 (51) 686 166
www.intechopen.com

InTech China
Unit 405, Office Block, Hotel Equatorial Shanghai
No.65, Yan An Road (West), Shanghai, 200040, China
中国上海市延安西路65号上海国际贵都大饭店办公楼405单元
Phone: +86-21-62489820
Fax: +86-21-62489821